Topological photonics: A mathematical perspective

Workshop Nonlinear Waves: “From Theoretical and Computational Advances to Experimental Observations”

ICERM

April 29, 2026

Alejandro Aceves

Department of Mathematics, Southern Methodist University

Topics

Topological photonics refers to designing properties of the propagating medium (photonic crystal fiber, waveguide lattice,..) in such a way that light propagates in unique and robust fashion.

- A brief tutorial on topological photonics
- Present work on transport and confinement in modulated photonic

Ross Prker, Currently: Researcher at the Center for Communications Research (CCR) in Princeton

A “zoology of optical” lattices
Topological photonics

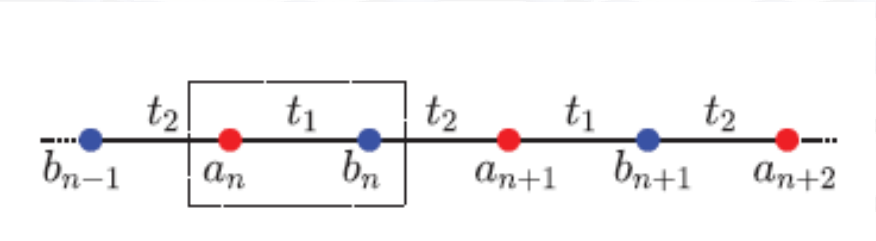

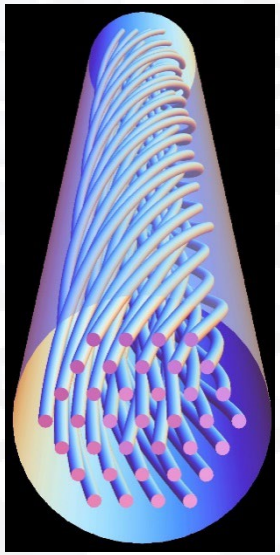

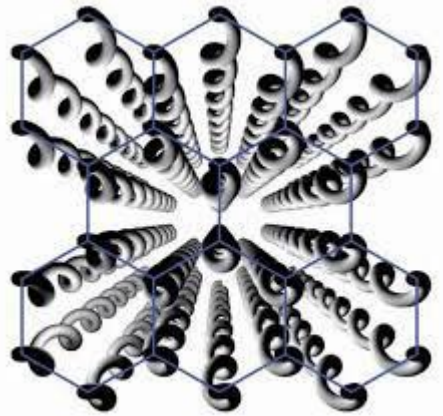

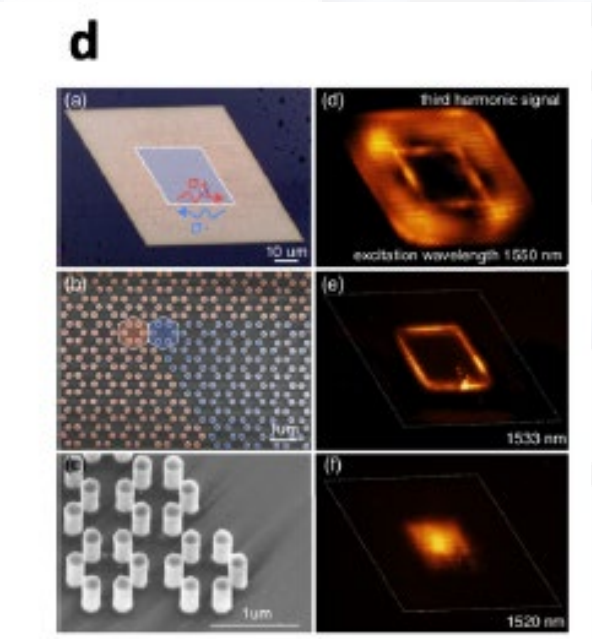

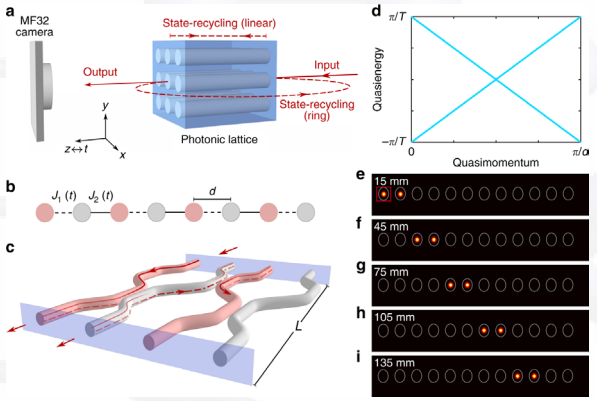

Programmable integrated photonics

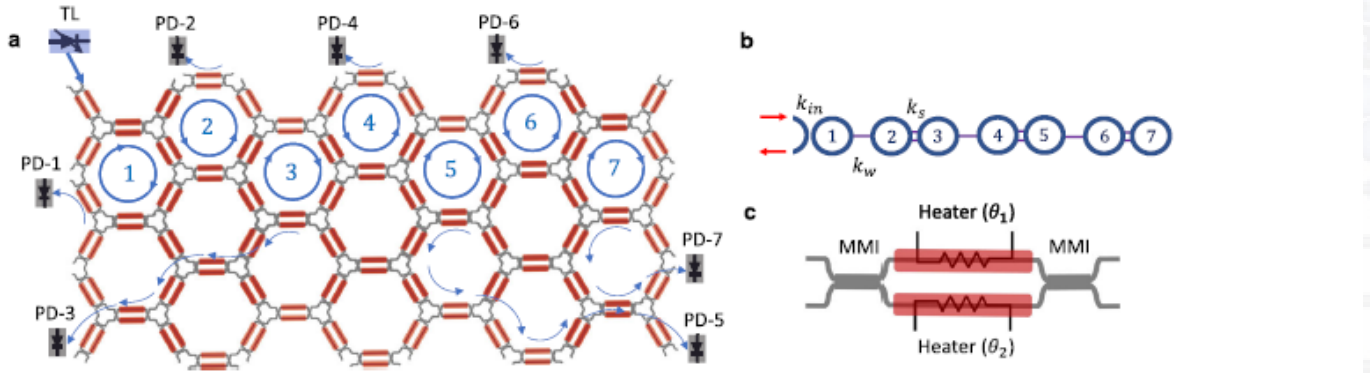

Fig. 1 | Programmable integrated photonics platform and implementation of the SSH model. **a** Schematic of the programmable mesh on iPronics' Smartlight Processor and reconfiguration for 7 coupled ring resonators; TL off-chip tunable laser, PD off-chip photodetector. **b** Implemented 1D SSH model. **c** Programmable unit cell in detail.

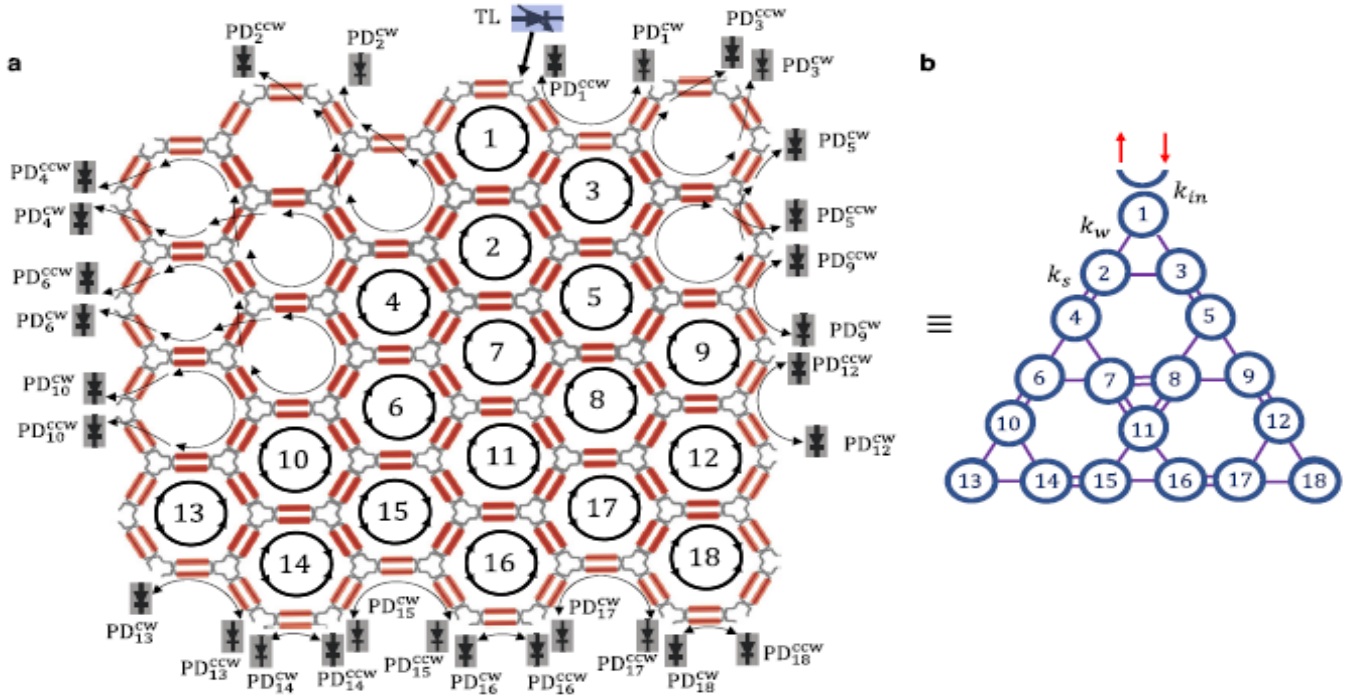

On, M.B., Ashtiani, F., Sanchez-Jacome, D. *et al.*
Programmable integrated photonics for topological Hamiltonians. *Nat Commun* **15**, 629 (2024)

One dimensional Su–Schrieffer-Heeger (SSH) lattice model

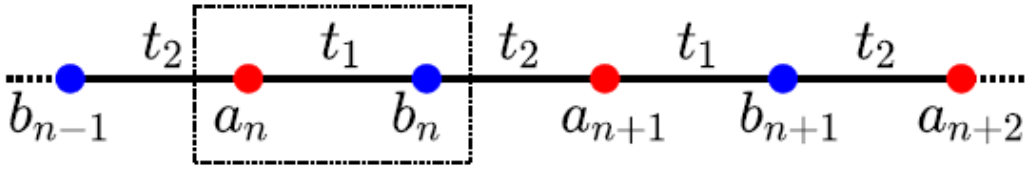

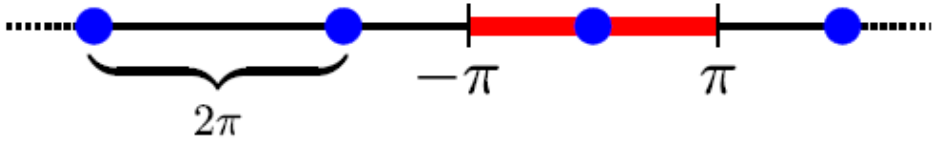

$$i\dot{a}_n + t_1 b_n + t_2 b_{n-1} + \gamma |a_n|^2 a_n = 0$$
$$i\dot{b}_n + t_1 a_n + t_2 a_{n+1} + \gamma |b_n|^2 b_n = 0,$$

"Discrete Breathers of Nonlinear Dimer Lattices: Bridging the Anti-continuous and Continuous Limits"
A Hofstrand, H Li, MI Weinstein ,Journal of Nonlinear Science, V.33 (59), (2023)

Linear model

$$i\dot{a}_n + t_1 b_n + t_2 b_{n-1} + \gamma |a_n|^2 a_n = 0$$

$$i\dot{b}_n + t_1 a_n + t_2 a_{n+1} + \gamma |b_n|^2 b_n = 0,$$

$$\mathbf{w}(k) = \begin{pmatrix} a_n \\ b_n \end{pmatrix} = \begin{pmatrix} a \\ b \end{pmatrix} e^{i(kn - \lambda t)},$$

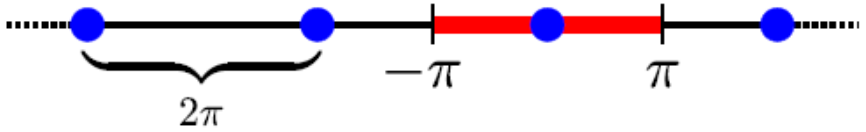

$$H(k)\underline{v} = -\lambda(k)\underline{v} \quad , \underline{v} = \begin{pmatrix} a \\ b \end{pmatrix}$$

$$H(k) = \begin{pmatrix} 0 & h(k) \\ h^*(k) & 0 \end{pmatrix}, \qquad h(k) = t_1 + t_2 e^{-ik}.$$

$$\lambda(k) = \pm |h(k)| = \sqrt{t_1^2 + t_2^2 + 2t_1 t_2 \cos k},$$

$$\lambda(k) = \pm|h(k)| = \sqrt{t_1^2 + t_2^2 + 2t_1 t_2 \cos k},$$

$$\mathbf{v}_\pm(k) = \frac{1}{\sqrt{2}} \begin{pmatrix} \pm e^{i\phi(k)} \\ 1 \end{pmatrix}$$

$$\tan\phi = \frac{\operatorname{Im} h(k)}{\operatorname{Re} h(k)} = -\frac{t_2 \sin k}{t_1 + t_2 \cos k}.$$

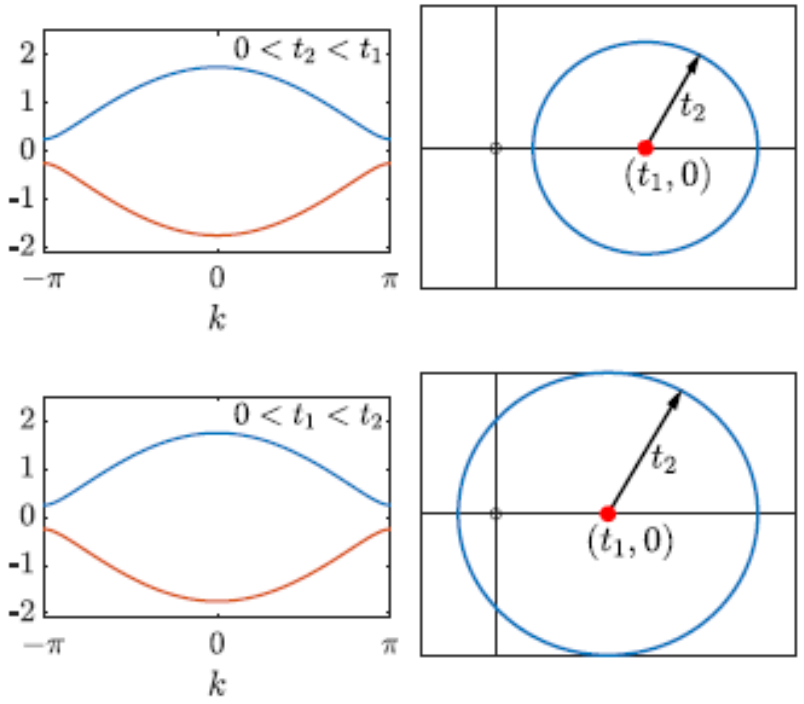

Figure 2: Left: band structure of the SSH model for $0 < t_2 < t_1$ (top) and $0 < t_1 < t_2$ (bottom). Right: circle in the complex plane traced counterclockwise by $h(k)$ for $k \in [-\pi, \pi]$.

$$\tan(\varphi) = -\frac{t_2 \sin(k)}{t_1 + t_2 \cos(k)}$$

Subtle but critical topological difference between t1 < t2 and t2 < t1

$$\mathrm{Ind}_h(0) = \begin{cases} -1 & t_1 < t_2 \\ 0 & t_1 > t_2 \end{cases}$$

Berry phase

We define the Berry connection by

$$A(k) = i\left\langle \mathbf{v}(k), \frac{d}{dk}\mathbf{v}(k) \right\rangle = i\mathbf{v}(k)^\dagger \frac{d}{dk}\mathbf{v}(k), \quad (11)$$

which is the coefficient of Δk on the RHS of (10). We then define the Berry phase to be the integral of Berry connection around a closed contour $\mathcal{C}$:

$$\gamma = \oint_{\mathcal{C}} A(k)dk. \quad (12)$$

$$\gamma = -\frac{1}{2}\int_{-\pi}^{\pi} \phi'(k)dk = \begin{cases} \pi & t_1 < t_2 \\ 0 & t_1 > t_2, \end{cases}$$

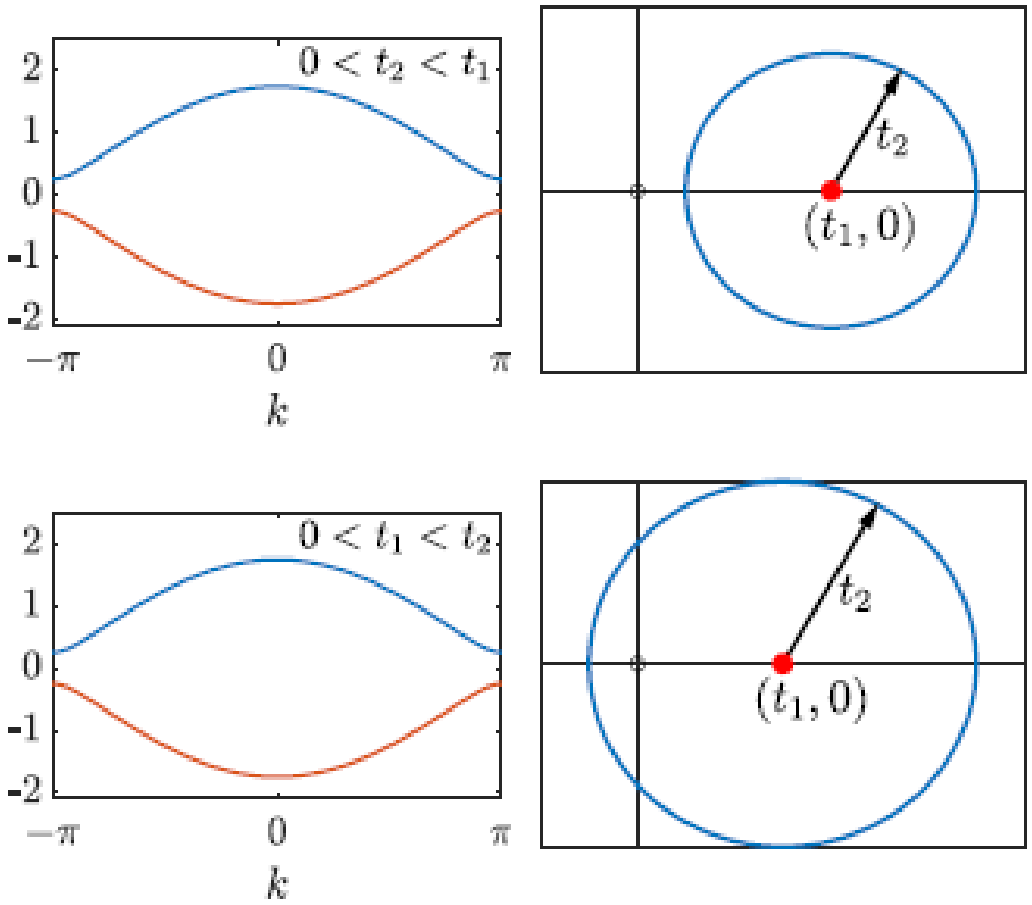

Figure 2: Left: band structure of the SSH model for $0 < t_2 < t_1$ (top) and $0 < t_1 < t_2$ (bottom). Right: circle in the complex plane traced counterclockwise by $h(k)$ for $k \in [-\pi, \pi]$.

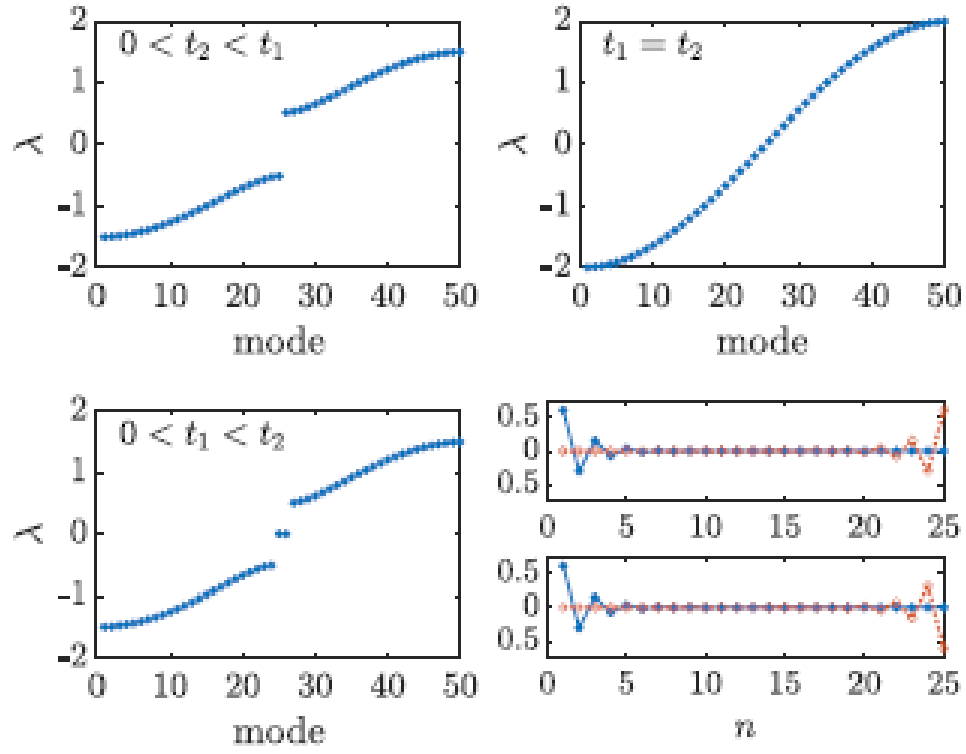

Effect of finite sites (Ex: N=25 sites)
Emergence of edge modes.

Picture of the Quantum Hall effect

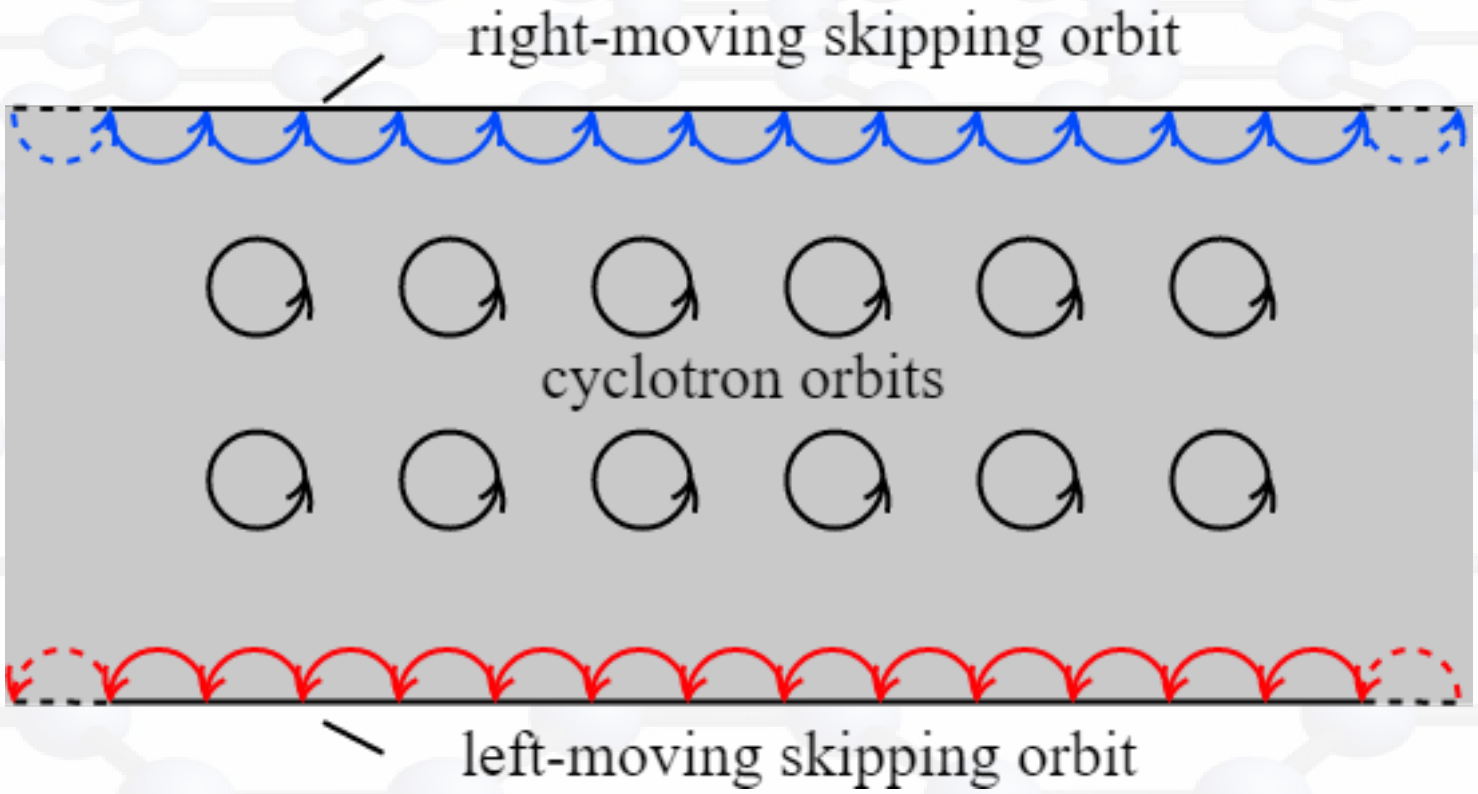

Two dimensional Haldane lattice models

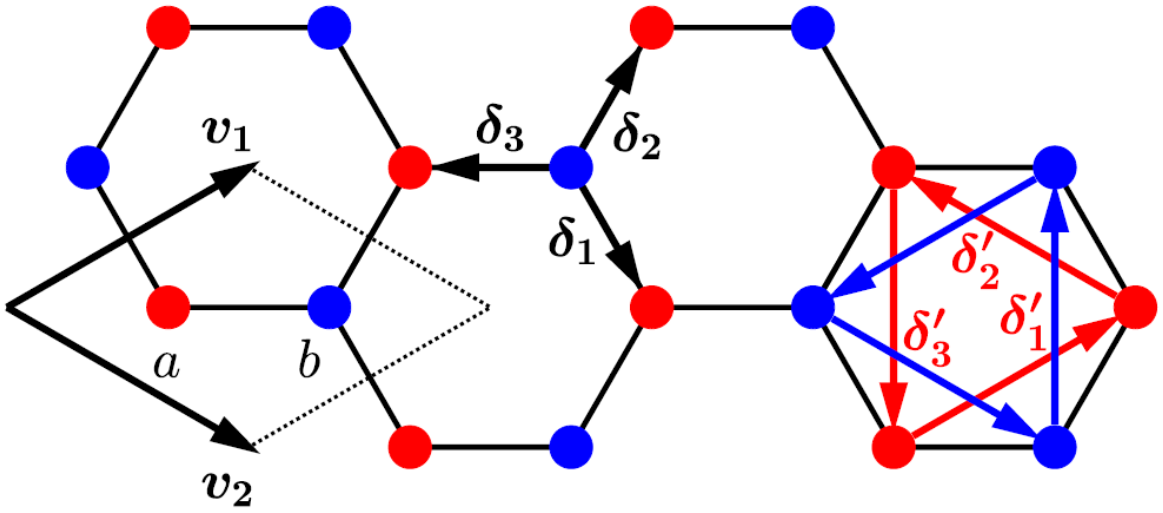

$$i\dot{a}_{\mathbf{n}} + t_0 a_{\mathbf{n}} + t_1 \sum_{\langle \mathbf{m} \rangle} b_{\mathbf{m}} \pm i t_2 \sum_{\langle\langle \mathbf{m} \rangle\rangle} a_{\mathbf{m}} = 0$$

$$i\dot{b}_{\mathbf{n}} - t_0 b_{\mathbf{n}} + t_1 \sum_{\langle \mathbf{m} \rangle} a_{\mathbf{m}} \pm i t_2 \sum_{\langle\langle \mathbf{m} \rangle\rangle} b_{\mathbf{m}} = 0,$$

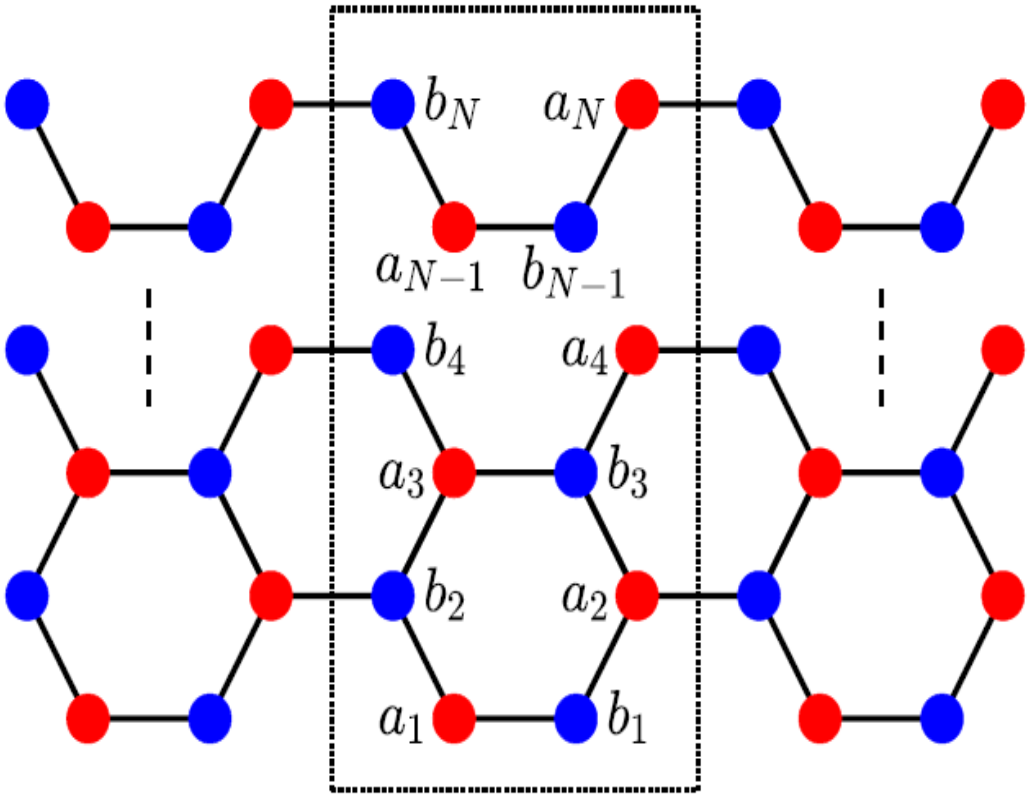

Floquet bands from Haldane type 2d models.

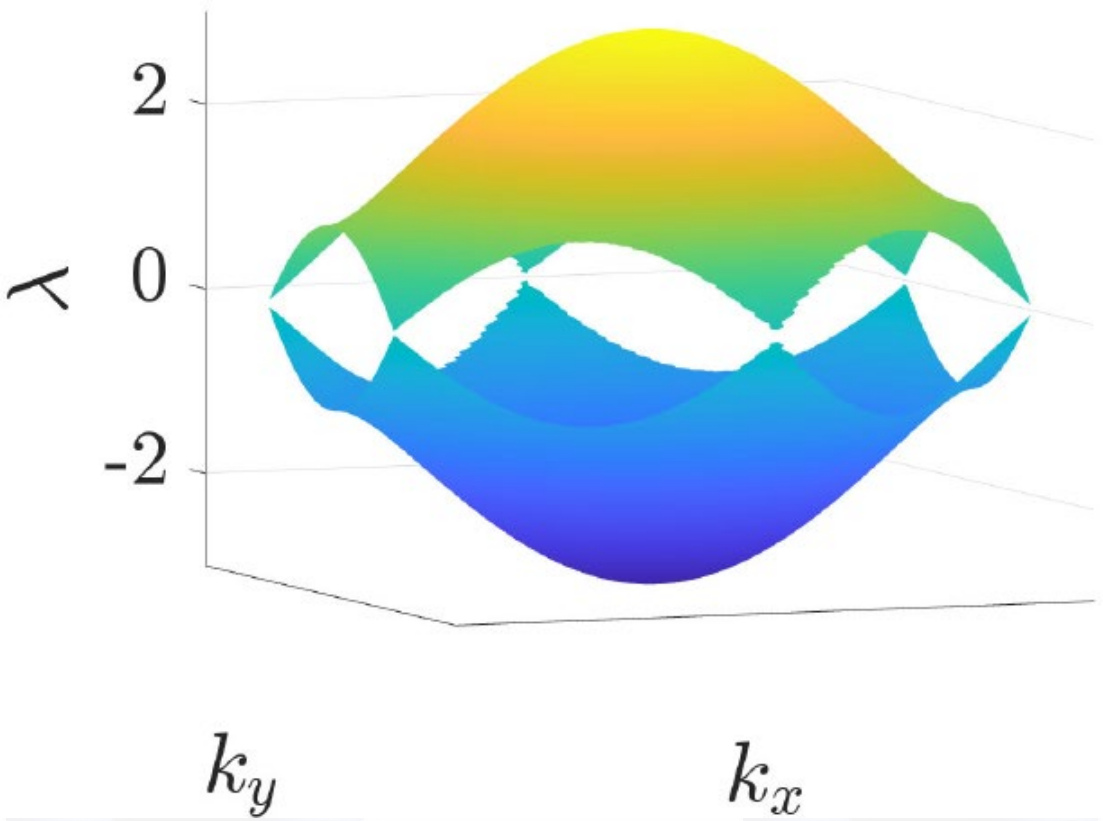

Plot shows imaginary part of Floquet exponents over the first Brillouin zone

Ross Parker, AA, “Topological Photonics: A Mathematical Perspective”, Notices of the American Mathematical Society 71(8), September 2024

Part 2: Periodic modulation of a photonic structure:

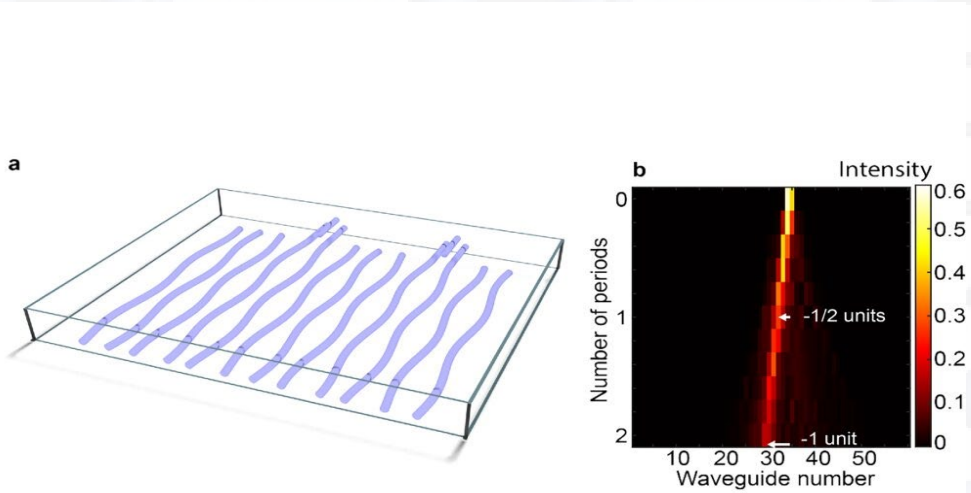

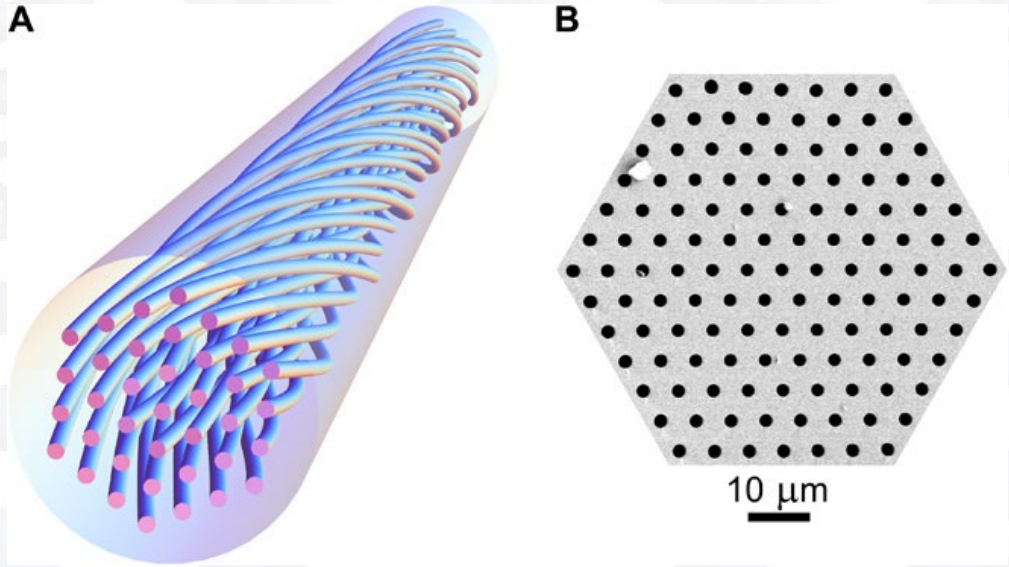

Mobility (Rechtman's talk)

Mode confinement from helicity
(Motivated by Russel's experiments)

Model studied (**non adiabatic. Seeking traveling wave solutions**)

$$i\frac{1}{L}\frac{du_n}{dZ} + J_n(Z)u_{n+1} + J_{n-1}(Z)u_{n-1} + g|u_n|^2 u_n = 0$$

$$J_n(Z) = J_0 + C\cos^2\left(\pi Z + \frac{4\pi}{3}n + \frac{\pi}{6}\right).$$

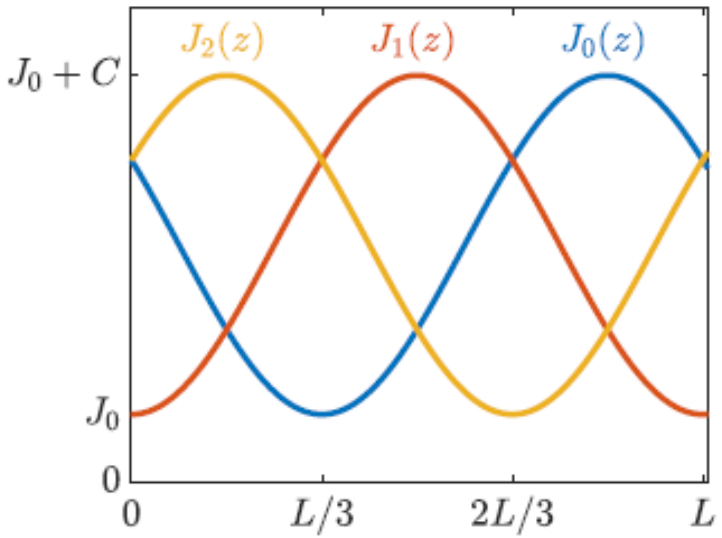

FIG. 1: Coupling functions $J_0(z)$, $J_1(z)$, and $J_2(z)$ of z-dependent nearest-neighbor couplings over one spatial period L.

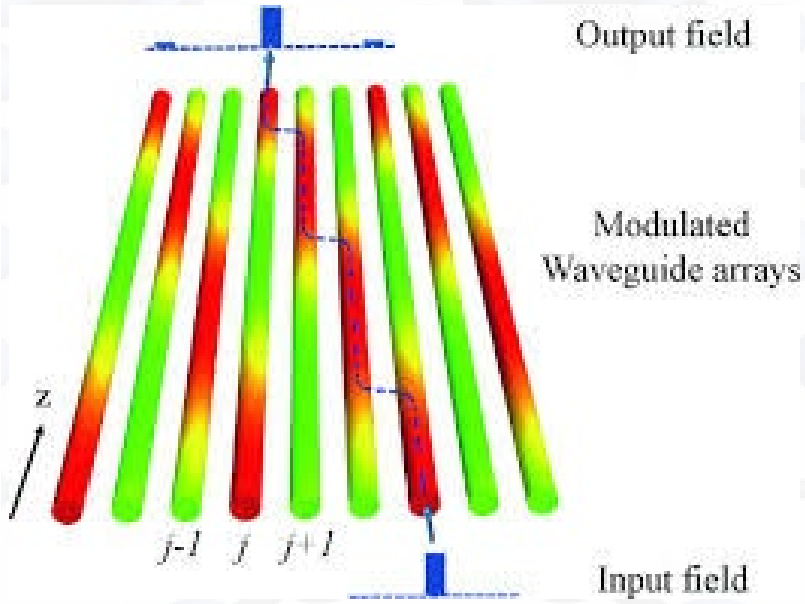

- Marius Jurgensen, Sebabrata Mukherjee, and Mikael C. Rechtsman, "Quantized nonlinear Thouless pumping",Nature 596 (2021), no. 7870, 63–67.
- Ross Parker, Alejandro Aceves, Jesús Cuevas-Maraver, and P. G. Kevrekidis Phys. Rev. E 108, 024214 – (2023)

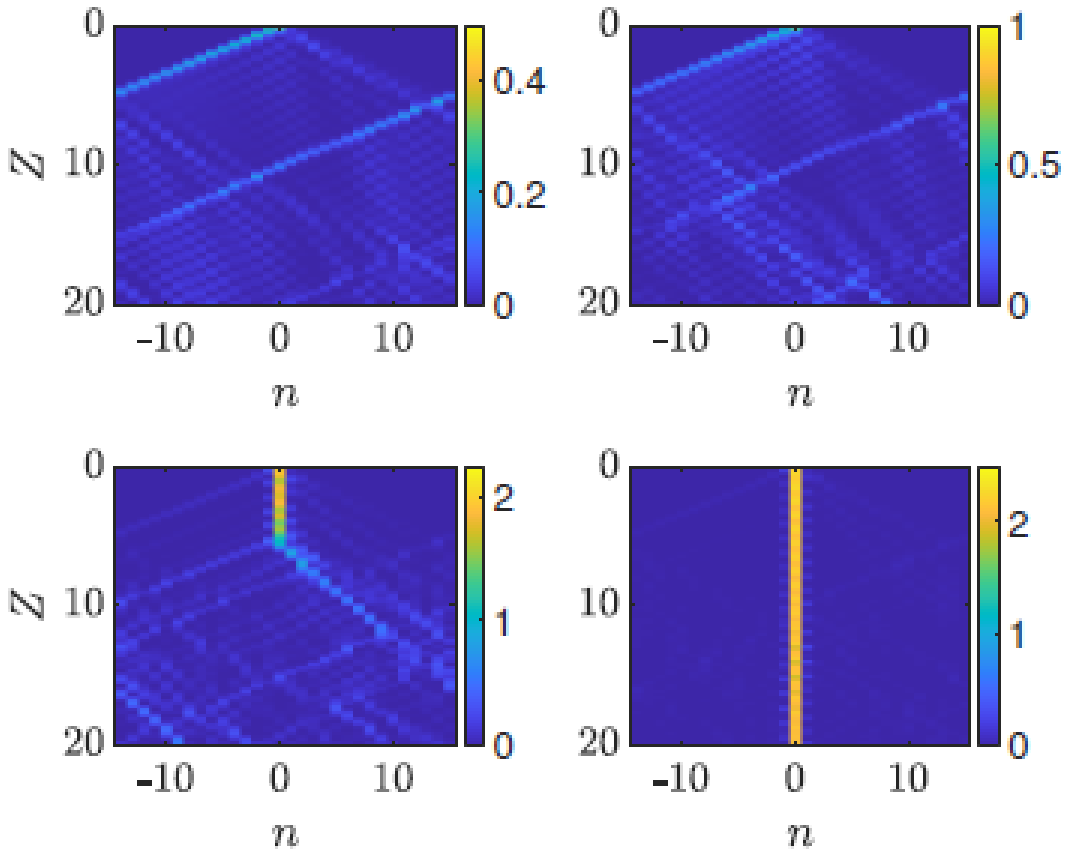

FIG. 2: Colormap showing the intensity of the solution of equation (5) evolving in Z, starting with a single excited site at $n = 0$ with intensity $P = 0.5, 1, 2.25, 2.5$ (left to right, top to bottom).

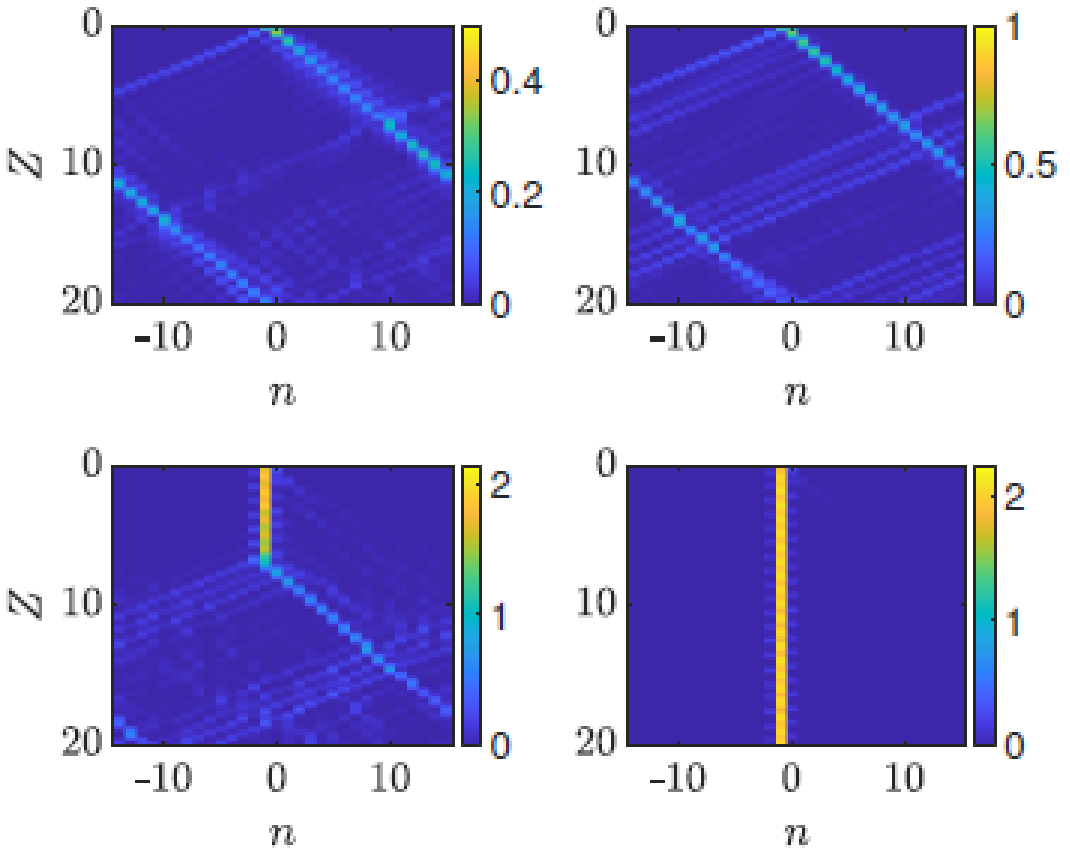

FIG. 3: Colormap showing the intensityf of the solution of equation (5) evolving in Z, starting with a single excited site at $n = -1$ with intensity $P = 0.5, 1, 2.15, 2.25$ (left to right, top to bottom).

Simplified Model

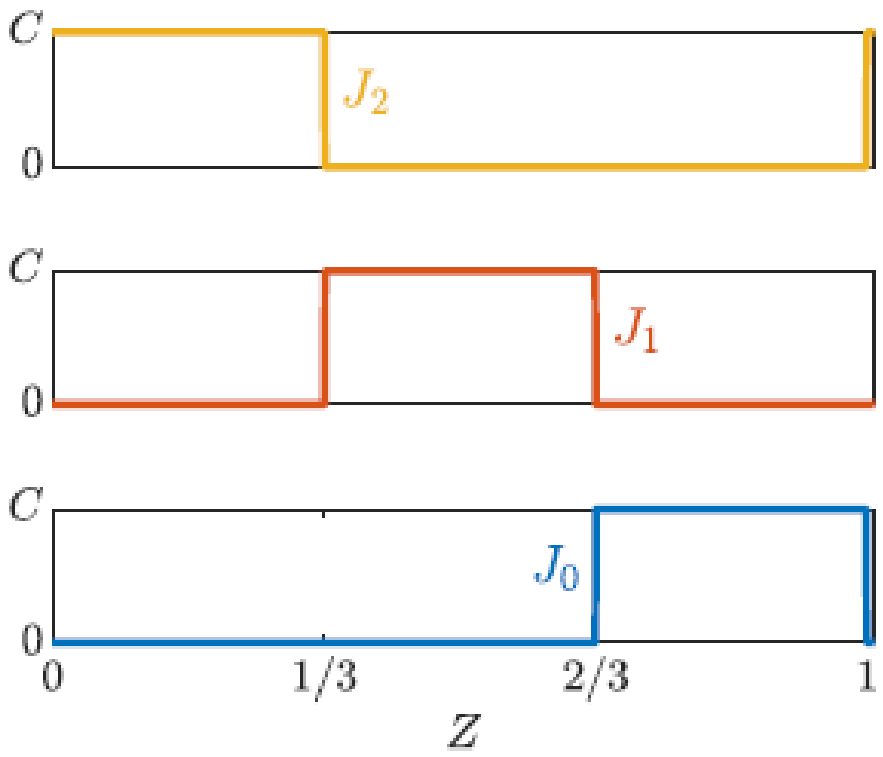

$$i\frac{1}{L}\frac{du_n}{dZ} + J_n(Z)u_{n+1} + J_{n-1}(Z)u_{n-1} + g|u_n|^2 u_n = 0$$

$$J_n(Z) = J_0 + C\cos^2\left(\pi Z + \frac{4\pi}{3}n + \frac{\pi}{6}\right).$$

Replace $J_n(Z)$ *by piecewise* $mod(3)$*constant funtions*

Simplified Model, II

$$\frac{d\rho_{0,0}}{dZ} = iLC\left(\rho_{-1,0} - \rho_{0,-1}\right)$$

$$\frac{d\rho_{-1,-1}}{dZ} = iLC\left(\rho_{0,-1} - \rho_{-1,0}\right)$$

$$\frac{d\rho_{-1,0}}{dZ} = iL\left[C(\rho_{0,0} - \rho_{-1,-1}) + g(\rho_{-1,-1} - \rho_{0,0})\rho_{-1,0}\right]$$

$$\frac{d\rho_{0,-1}}{dZ} = iL\left[C(\rho_{-1,-1} - \rho_{0,0}) + g(\rho_{0,0} - \rho_{-1,-1})\rho_{0,-1}\right].$$

$$\rho_{nm} = \overline{\rho_{mn}} = \overline{u_n}u_m$$
$$\rho_{nn} = |u_n|^2$$

Simplified Model III

Define: $p = \rho_{0,0} - \rho_{-1,-1}$, $q = i(\rho_{-1,0} - \rho_{0,-1})$, $r = \rho_{-1,0} - \rho_{0,-1}$

Results in:

$$\frac{dp}{dZ} = 2LCq$$

$$\frac{dq}{dZ} = -L(2Cp\text{-gpr})$$

$$\frac{dr}{dZ} = -Lgpq$$

$$r - r_0 = \frac{g}{4c}(p^2 - p_0^2),$$

$$\frac{d^2p}{dZ^2} = L(Ap - Bp^3)$$

$$p(Z) = \begin{cases} P\,\mathrm{cn}\left(2CLZ; k = \frac{gP}{4C}\right) & P < P^* \\ P\,\mathrm{dn}\left(\frac{gPL}{2}Z; k = \frac{4C}{gP}\right) & P > P^*, \end{cases} \quad P^* = \frac{4C}{g}$$

$$|u_0(Z)|^2 = \frac{1}{2}(P + p(Z)) \qquad |u_{-1}(Z)|^2 = \frac{1}{2}(P - p(Z))$$

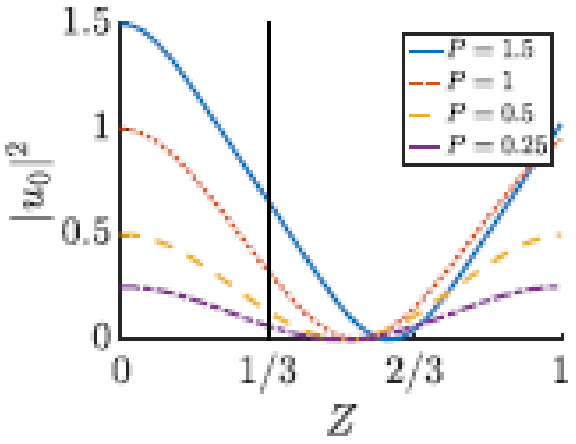

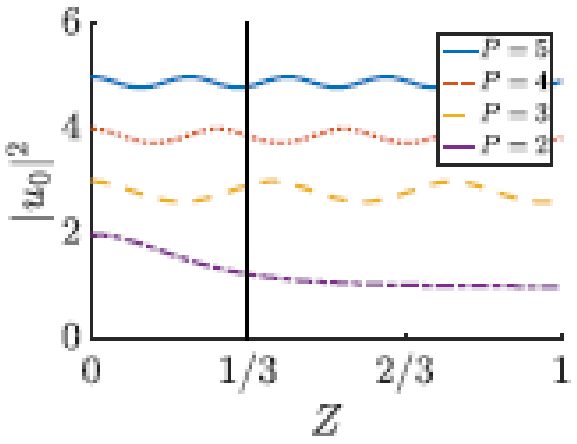

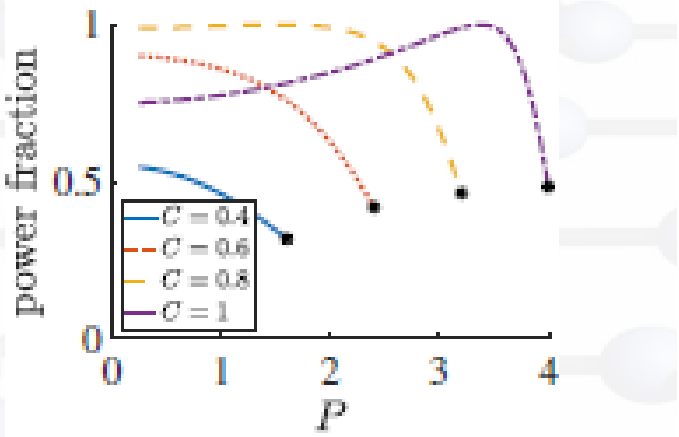

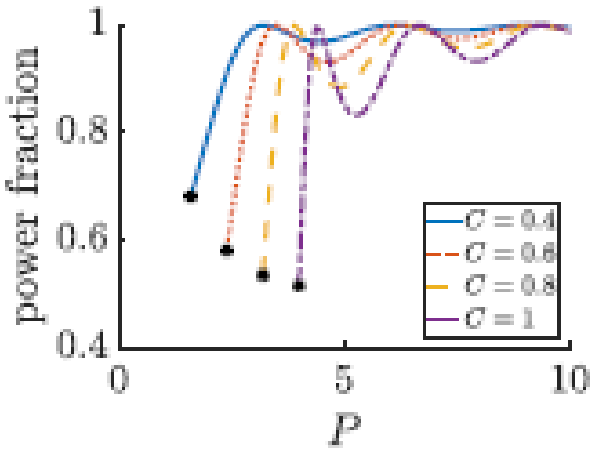

Power transfer n=0 to n=-1
At Z=1/3, P < P*

Power kept at n=0
At Z=1/3, P > P*

Simplified model

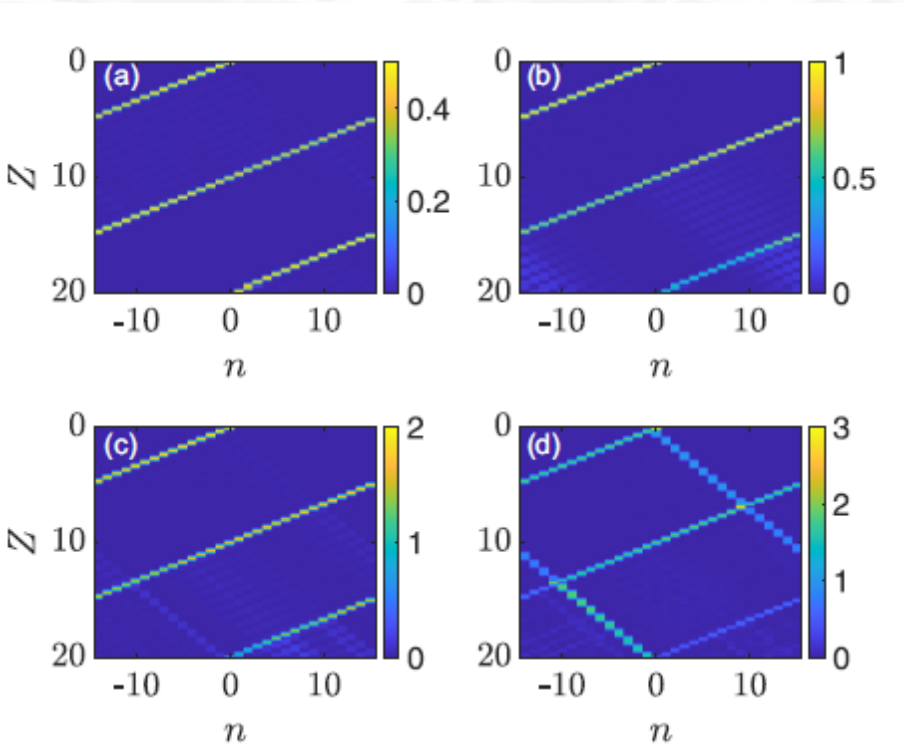

FIG. 7. Colormap showing the intensity of the solution of Eq. (5) with the simplified coupling function Eq. (10) for $P < P^*$ evolving in Z, starting with a single excited site at $n = 0$ with intensity (a) $P = 0.5$, (b) $P = 1$, (c) $P = 2$, and (d) $P = 3$. The fraction of intensity transferred from site $n = 0$ to site $n = -1$ at $Z = \frac{1}{3}$ is (a) 0.9910, (b) 0.9959, (c) 0.9909, and (d) 0.6636. The other parameters are $P^* = 3.2$, $C = 0.8$, and $g = 1$.

P < P* , C =0.8

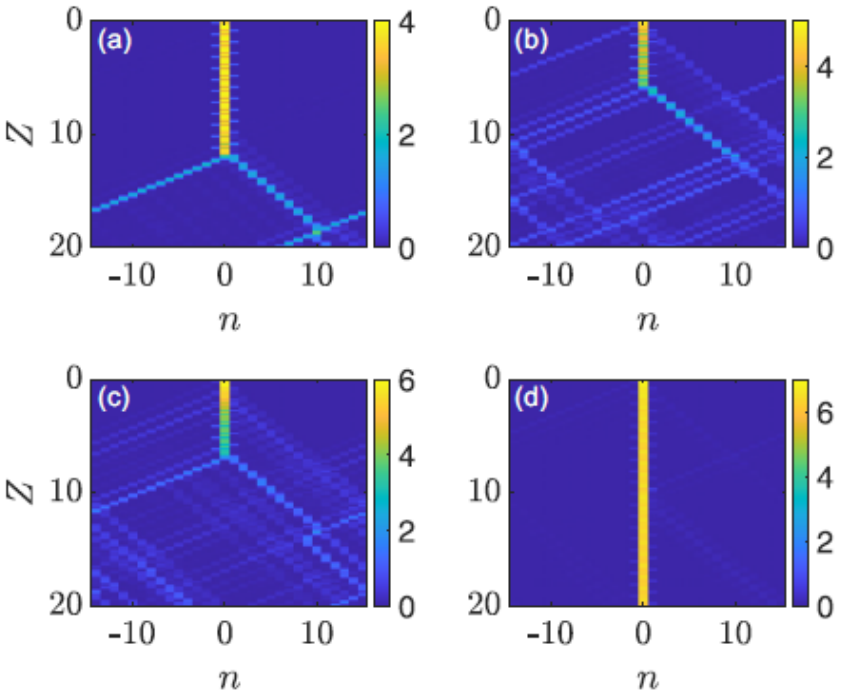

FIG. 10. Colormap showing the intensity of the solution of Eq. (5) with the simplified coupling function Eq. (10) for $P > P^*$ evolving in Z, starting with a single excited site at $n = 0$ with intensity (a) $P = 4$, (b) $P = 5$, (c) $P = 6$, and (d) $P = 7$. The fraction of intensity remaining at site $n = 0$ at $Z = \frac{1}{3}$ is (a) 0.9938, (b) 0.8853, (c) 0.9815, and (d) 0.9797. The other parameters are $P^* = 3.2$, $C = 0.8$, and $g = 1$.

P > P* , C =0.8

Exact traveling wave and stationary solutions

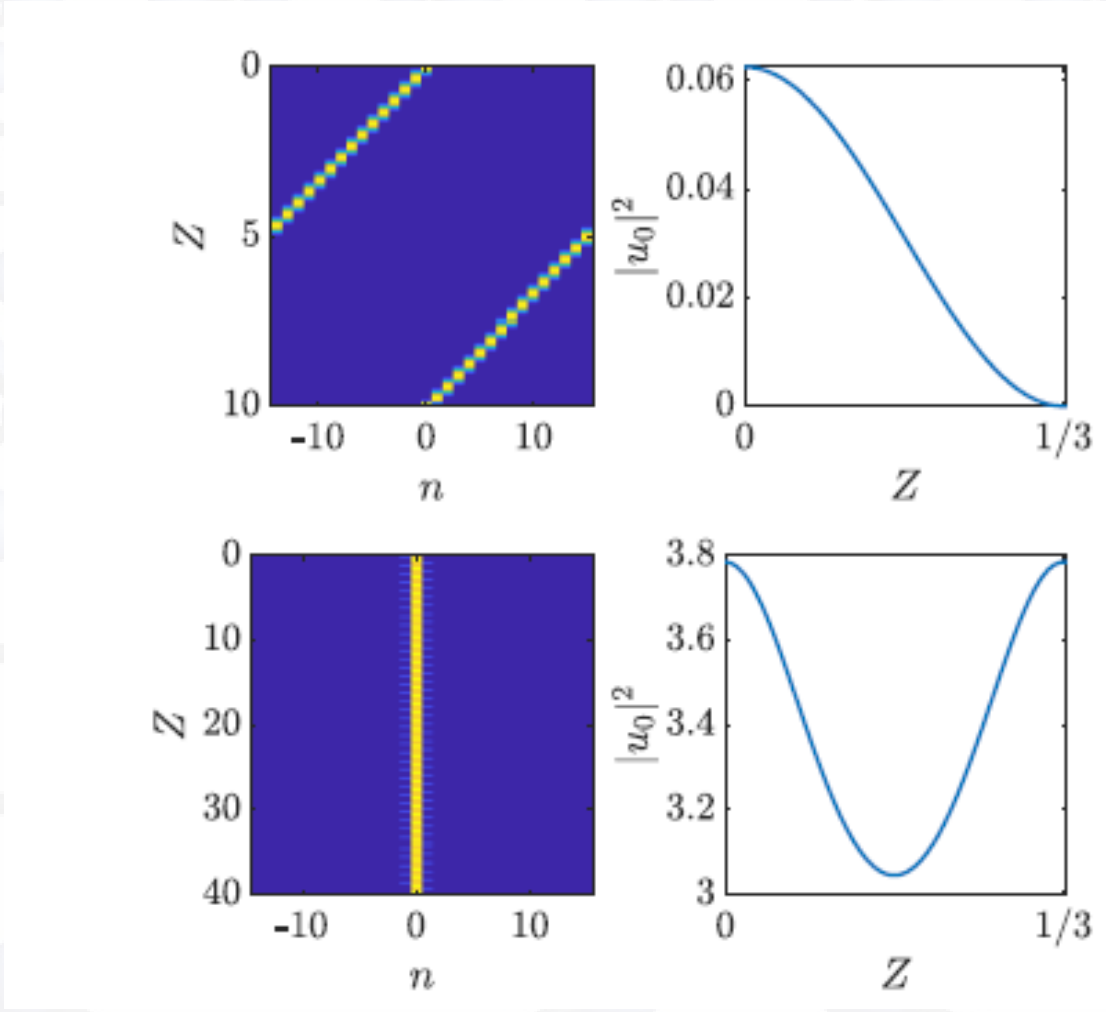

Exact model

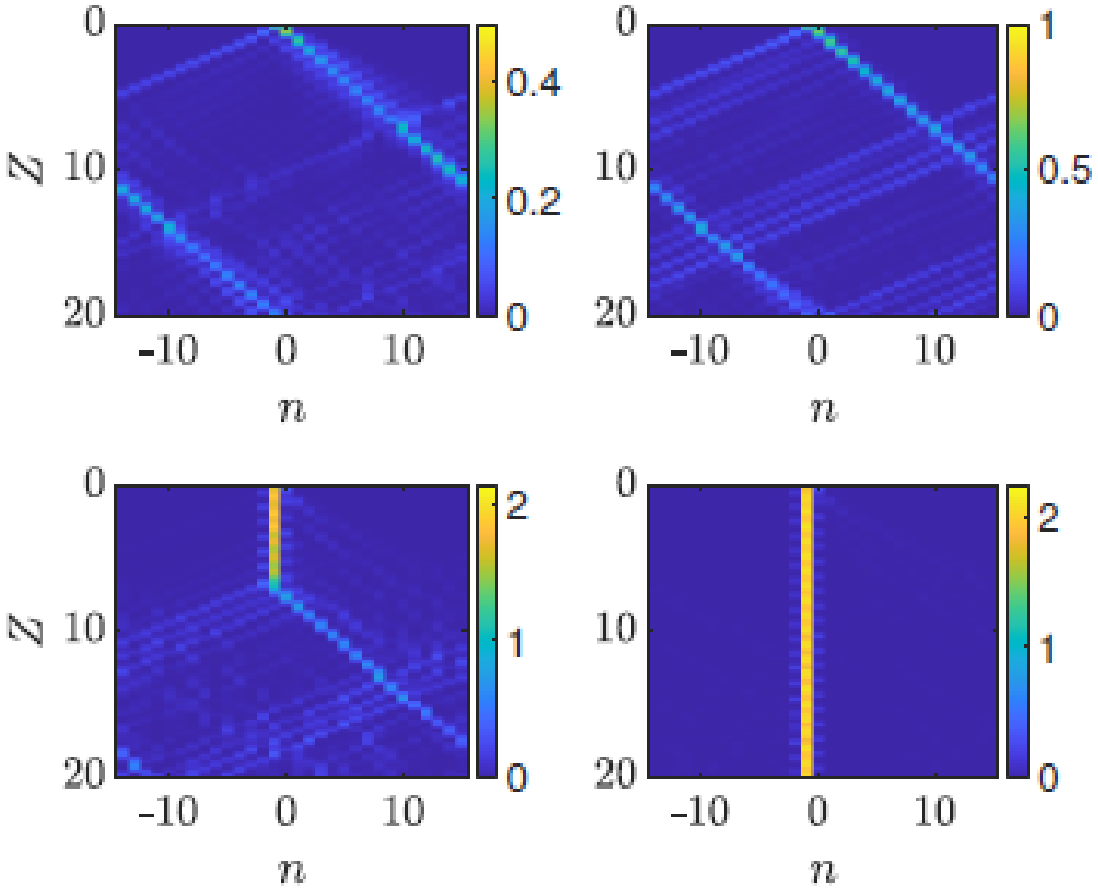

FIG. 3: Colormap showing the intensityf of the solution of equation (5) evolving in Z, starting with a single excited site at $n = -1$ with intensity $P = 0.5, 1, 2.15, 2.25$ (left to right, top to bottom).

Simplified model

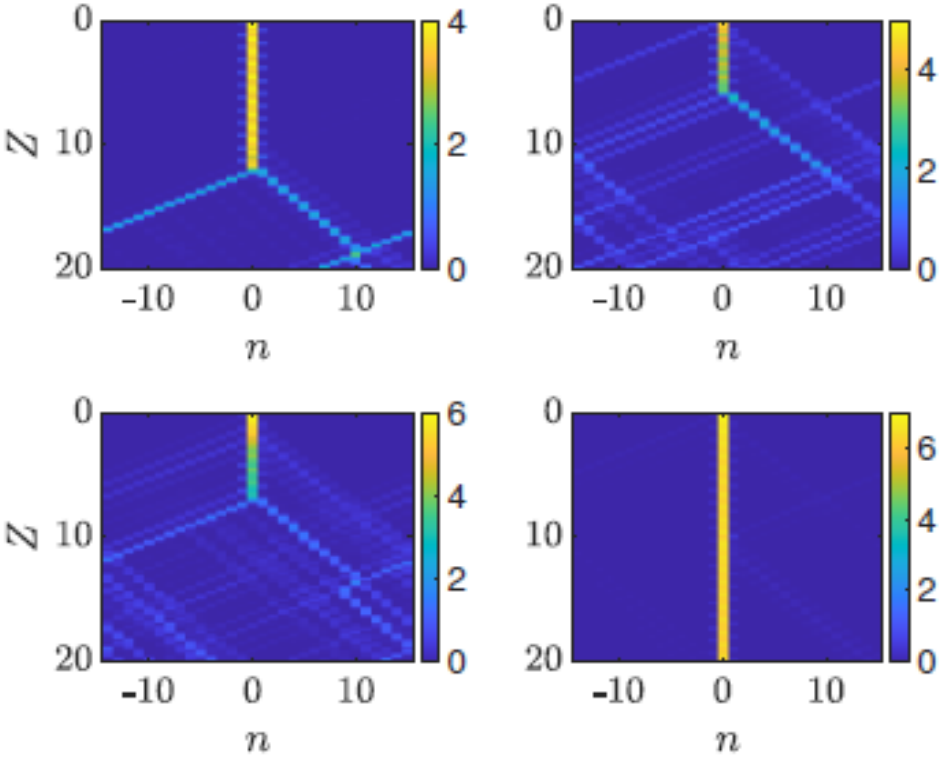

FIG. 10: Colormap showing intensity of the solution of equation (5) with simplified coupling function (10) evolving in Z, starting with a single excited site at $n = 0$ with intensity $P = 4, 5, 6, 7$, $P > P^*$ (left to right, top to bottom). Fraction of intensity remaining at site $n = 0$ at $Z = 1/3$ is 0.9938, 0.8853, 0.9815, and 0.9797 (respectively). $P^* = 3.2$, $C = 0.8$, $g = 1$.

Stationary solutions

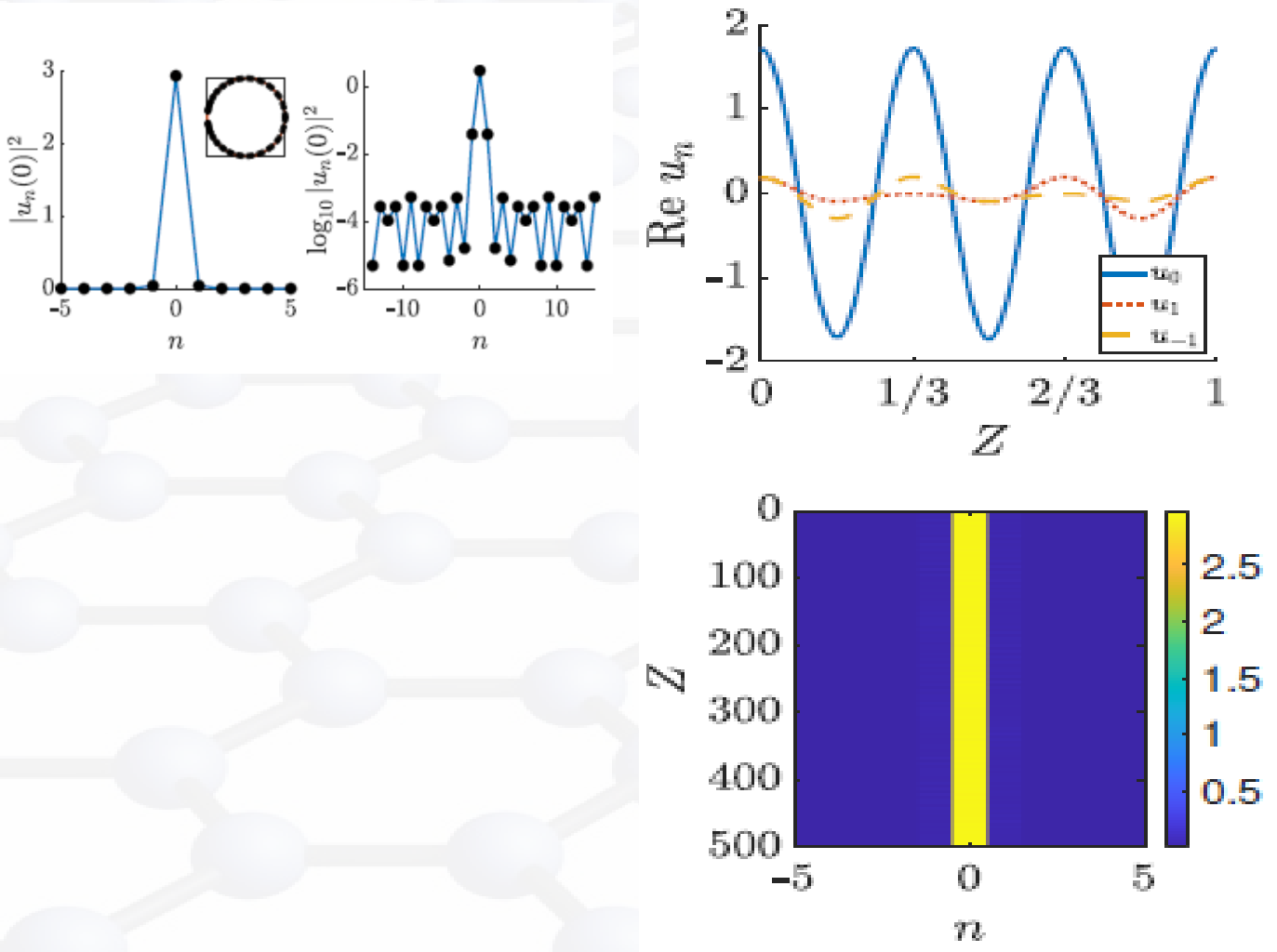

Traveling wave solutions

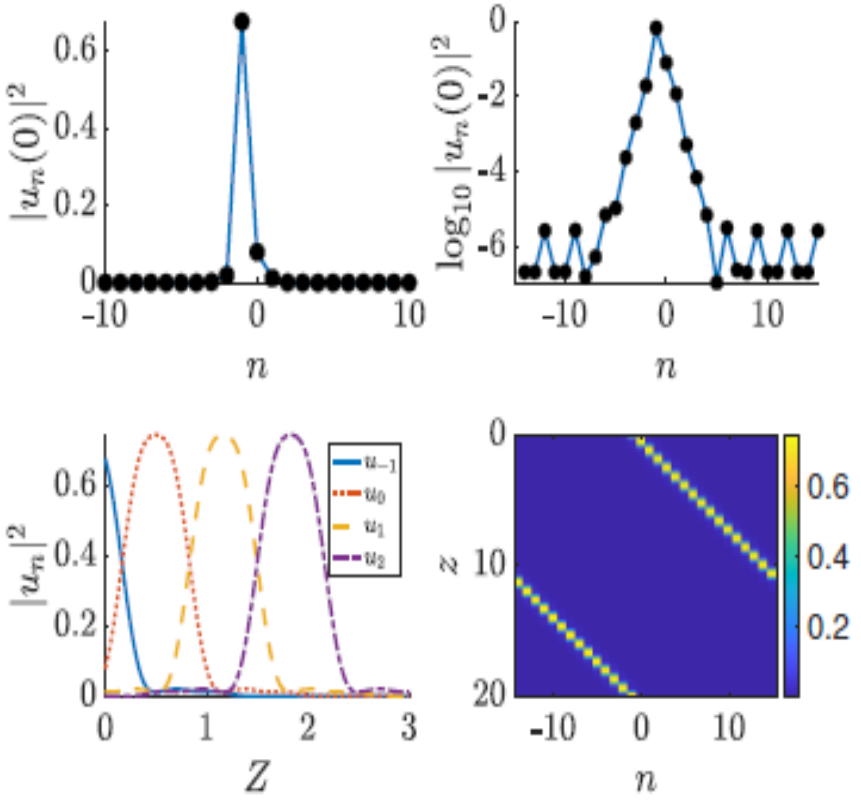

FIG. 18: Initial intensity $|u_n(0)|^2$ (top left) and log of initial intensity (top right) for right moving solution. The intensity of the solution evolved in Z over a period is presented for a few select sites (bottom left), and the space-time contour plot evolution of the intensity for the traveling wave is also shown (bottom right).

“Stationary” solutions, continuation approach

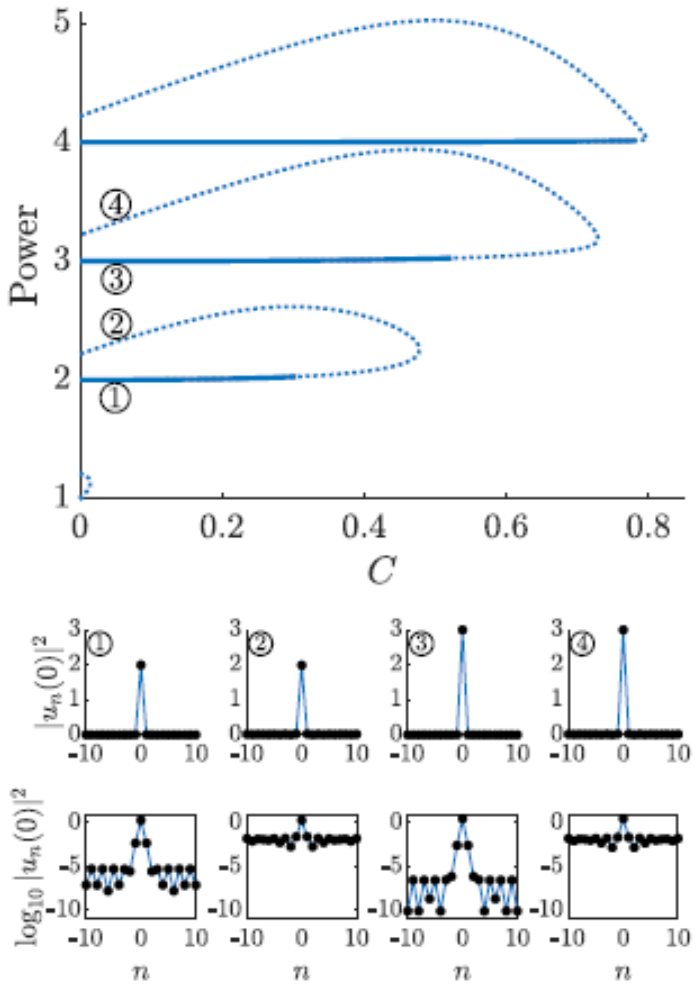

$$i\frac{1}{L}\frac{du_n}{dZ} + J_n(Z)u_{n+1} + J_{n-1}(Z)u_{n-1} + g|u_n|^2 u_n = 0$$

$$J_n(Z) = J_0 + C\cos^2\left(\pi Z + \frac{4\pi}{3}n + \frac{\pi}{6}\right).$$

Branches of stationary solutions with period (in Z) of 1, obtained from numerical parameter continuation starting with DNLS soliton at C = 0. Bottom plots show intensity (top) and log of the intensity (bottom) of initial condition, and correspond to C = 0.05 at labeled points on bifurcation diagram.

- Existence and tails of traveling wave solutions

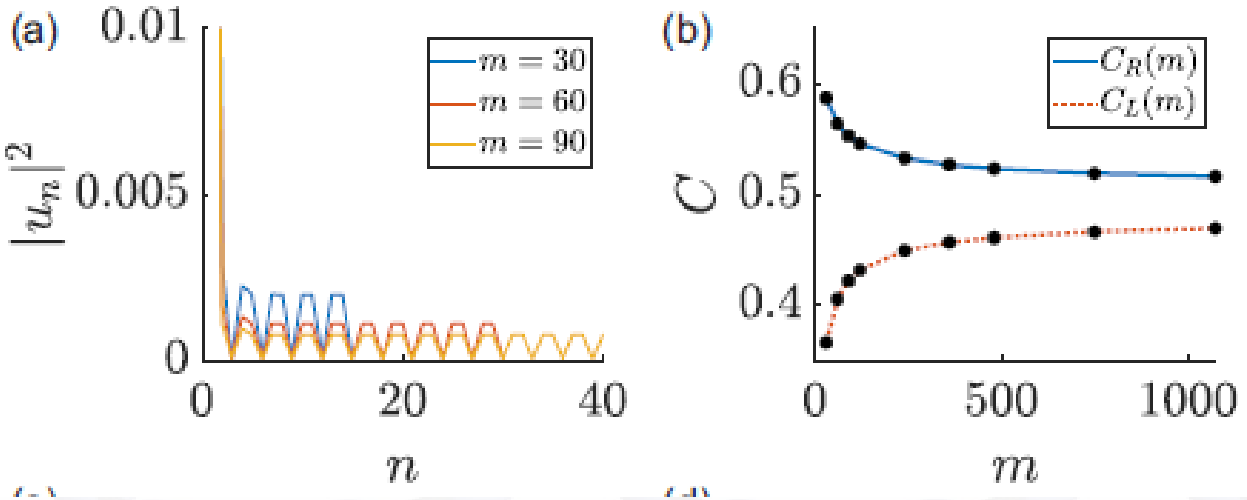

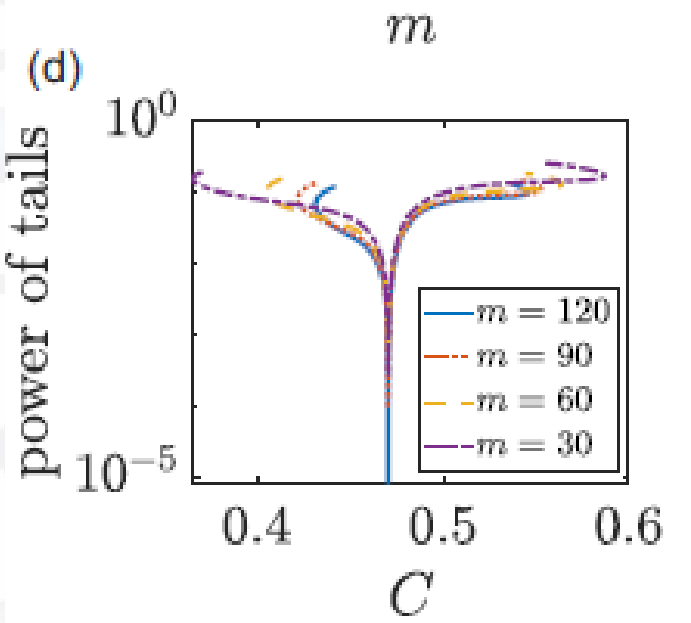

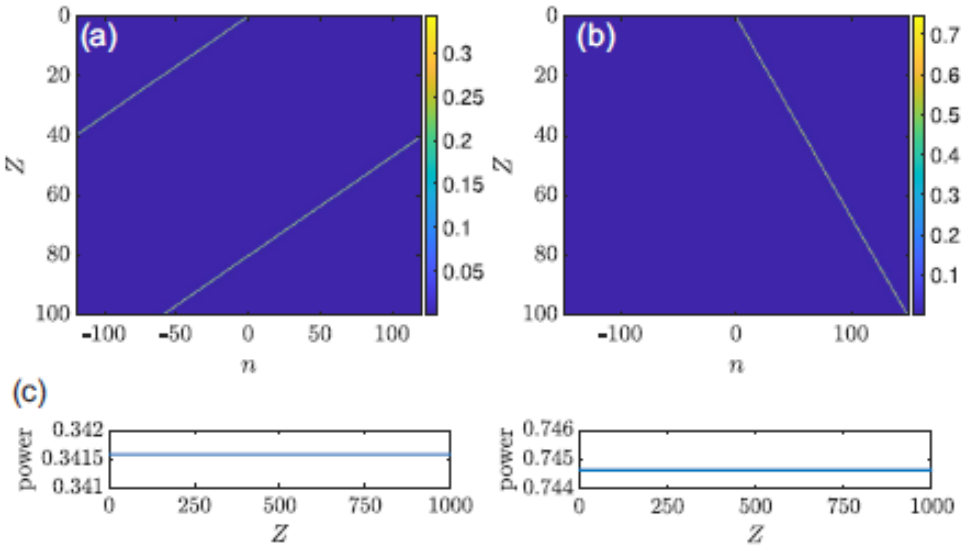

FIG. 20. Colormap of long-term evolution in Z of (a) the left-moving solution ($C = 0.4703$ and $m = 240$) and (b) the right-moving solution ($C = 0.5054$ and $m = 300$) for $C = C^*$. (c) Intensity of the site with a peak intensity of the moving solution over 1000 periods.

Experimental realization in a **non-adiabatic**, non-Hermitian model

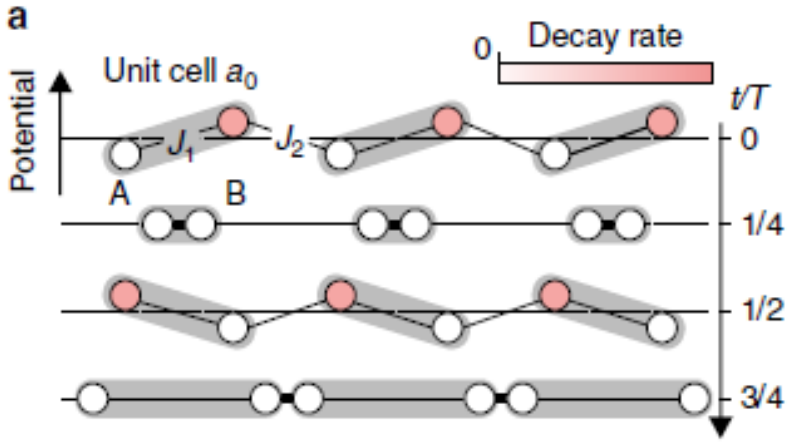

Non-Hermitian driven Rice-Mele model.

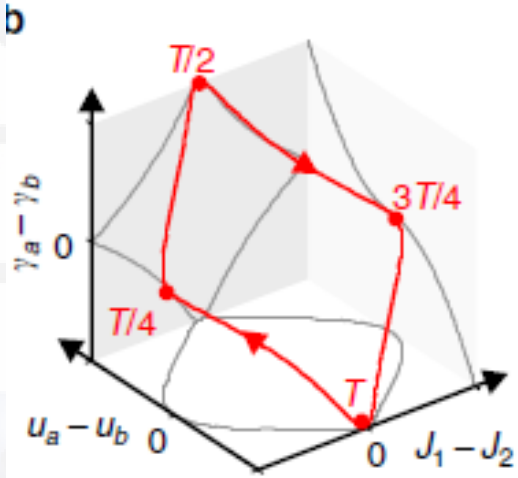

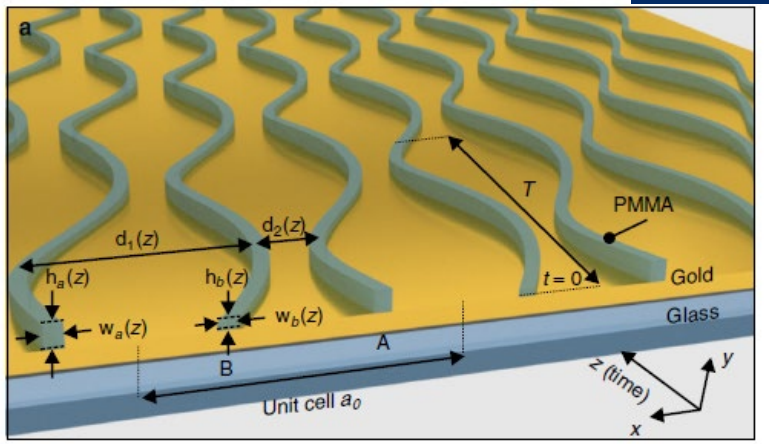

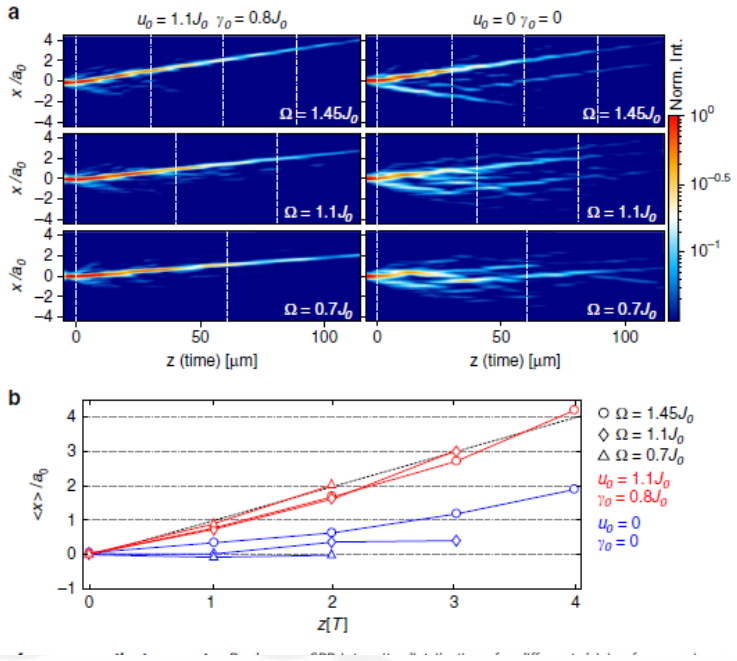

"Observation of topological transport quantization by dissipation in fast Thouless pumps", Zlata Fedorova, Haixin Qiu, Stefan Linden, Johann Kroha, NATURE COMMUNICATIONS (2020)

Twisted multicore waveguide arrays: Tunneling inhibition

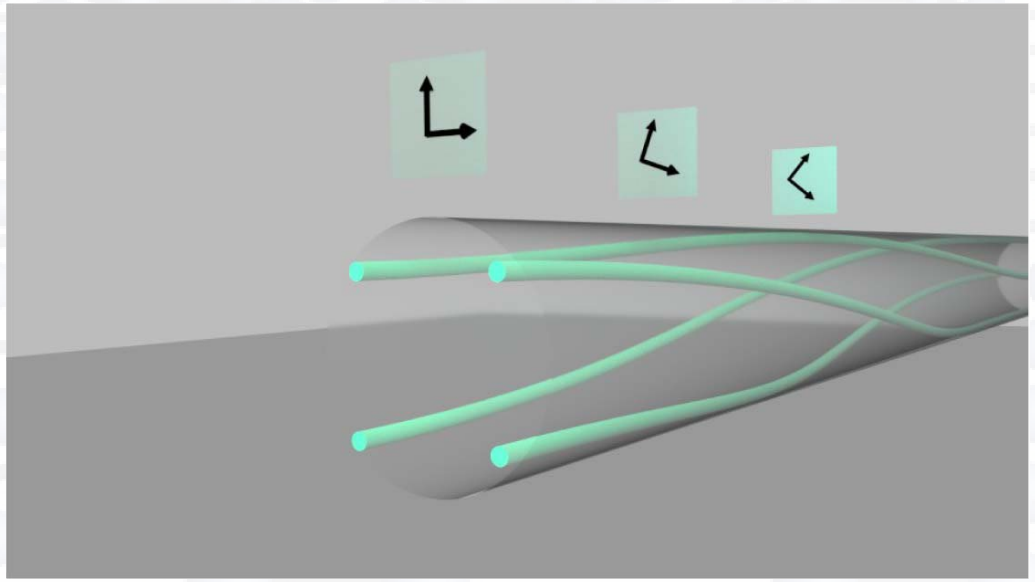

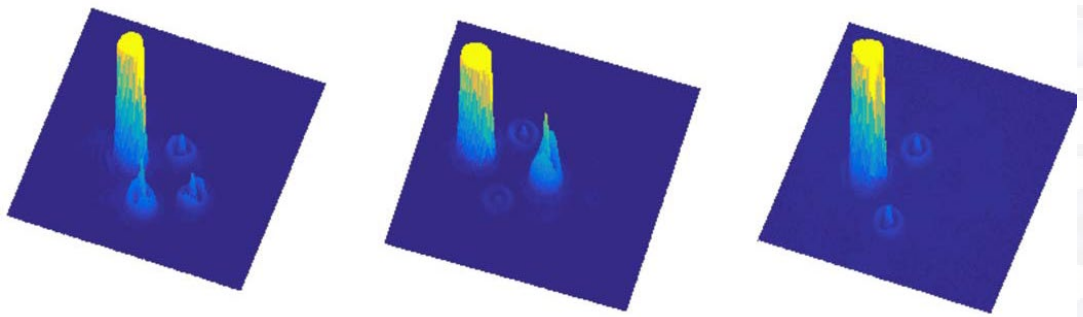

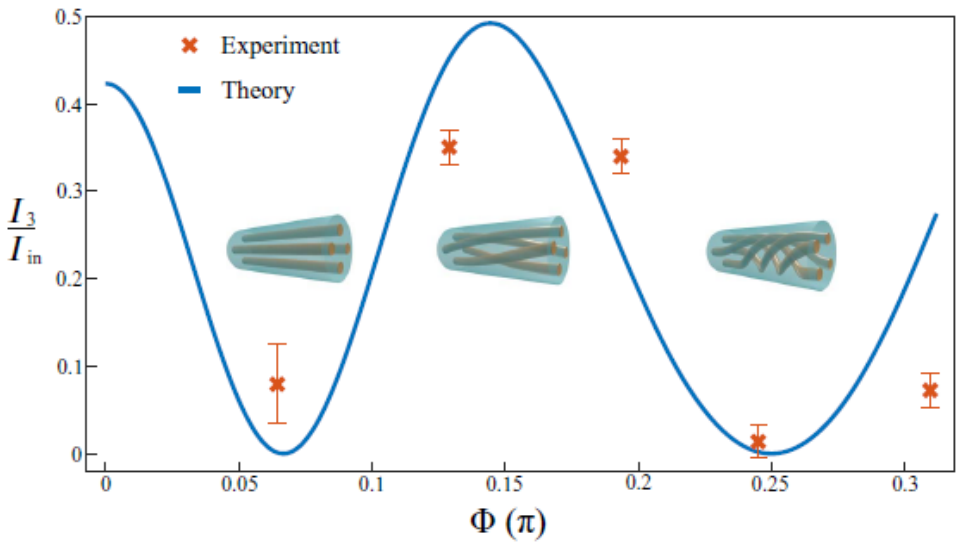

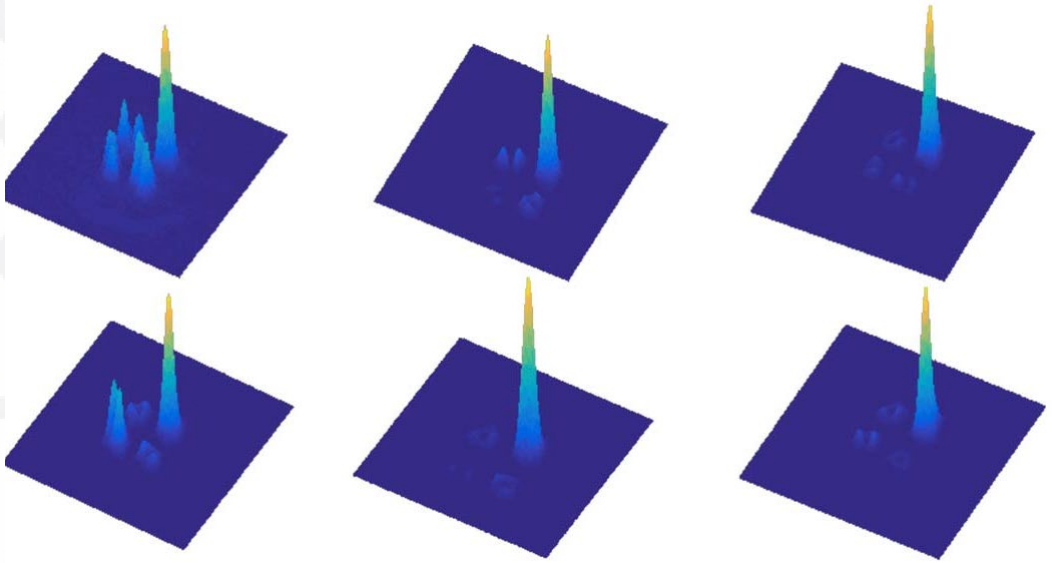

"Observation of twist-induced geometric phases and inhibition of optical tunneling via Aharonov-Bohm effects"
Midya Parto, et.al, Sci. Adv. 2019.

Twisted Light

From: "*Twist-induced guidance in coreless photonic crystal fiber: A helical channel for light*"

Ramin Beravat, Gordon K. L. Wong*, Michael H. Frosz, Xiao Ming Xi and Philip St.J. Russell

Science Advances 25 Nov 2016: Vol. 2, no. 11, e1601421
DOI: 10.1126/sciadv.1601421

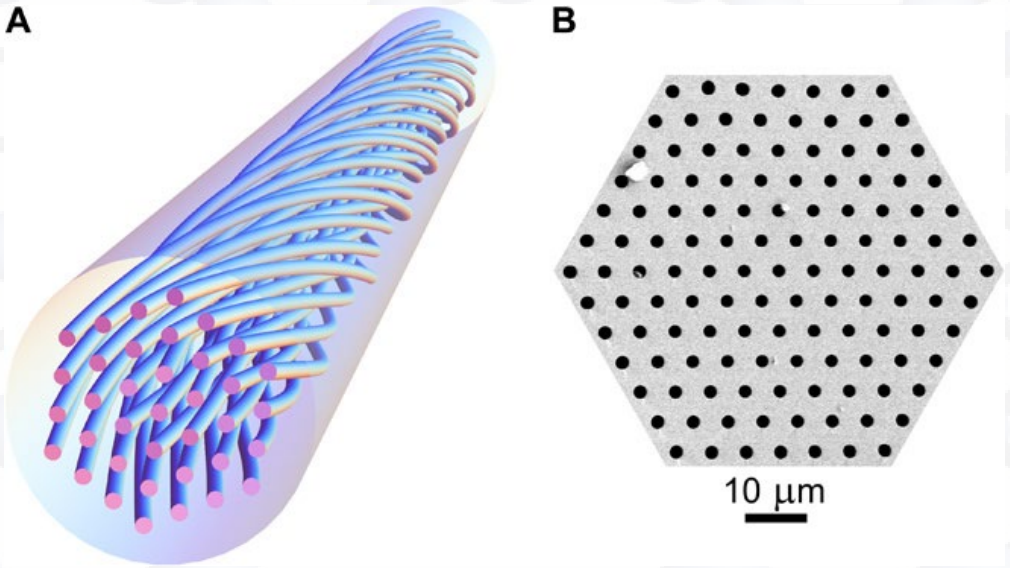

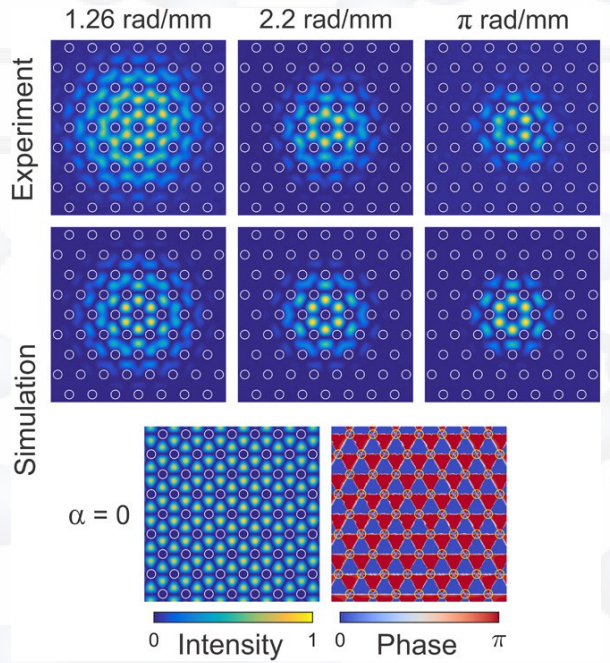

Mode confinement from helicity

"The resulting helically curved periodic "space" creates a topological channel within which light can be robustly trapped, with a confinement strength that scales with the twist rate"
"In the twisted fiber, these lobes are forced to describe helical paths around the fiber axis, which increases their effective axial refractive index in proportion to the square of the radius r"

Ray Theory

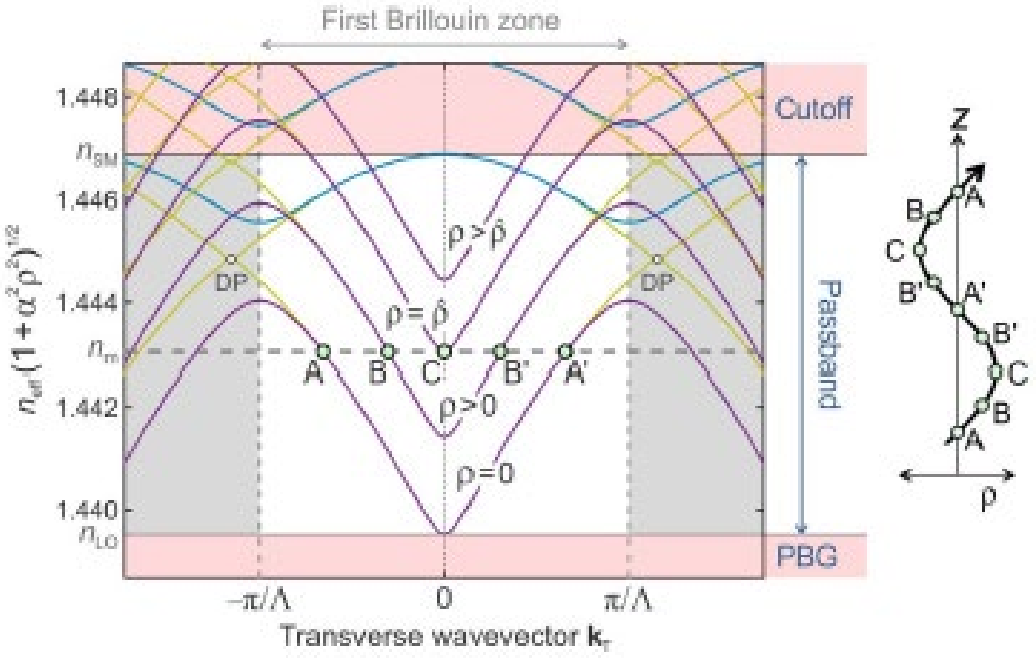

$$\frac{d\mathbf{x}}{d\sigma} = \nabla_{\mathbf{k}} H(\mathbf{k}, \mathbf{x}), \qquad \frac{d\mathbf{k}}{d\sigma} = \nabla_{\mathbf{x}} H(\mathbf{k}, \mathbf{x})$$

$$\partial(x, y, z, -ct)/\partial\sigma \approx (2Ak_x, 2Ak_y, -1, n_{LO})$$

$$\partial(k_x, k_y, k_z, \omega/c)/\partial\sigma = -\frac{\alpha^2 n_{LO}\omega}{c}(x, y, 0, 0)$$

$$\frac{d^2\mathbf{x}}{d\sigma^2} = [\nabla_{\mathbf{k}}\nabla_{\mathbf{k}} H] \otimes (-\nabla_{\mathbf{x}} H) = [1/m^*] \otimes \mathbf{F}$$

$$\hat{\rho} = \alpha^{-1}\sqrt{(n_m/n_{LO})^2 - 1}$$

$$H = -k_z + (1 + \alpha^2\rho^2/2)\omega n_{LO}/c + A(k_x^2 + k_y^2) = 0$$

$$(\ddot{x}, \ddot{y}) = -(x, y)(\alpha^2 2\omega c A/n_{LO}) = -(x, y)\Omega^2$$

"*Twist-induced guidance in coreless photonic crystal fiber: A helical channel for light*" Ramin Beravat, Gordon K. L. Wong*, Michael H. Frosz, Xiao Ming Xi and Philip St.J. Russell Science Advances 25 Nov 2016: Vol. 2, no. 11, e1601421 DOI: 10.1126/sciadv.1601421

Kapitza pendulum

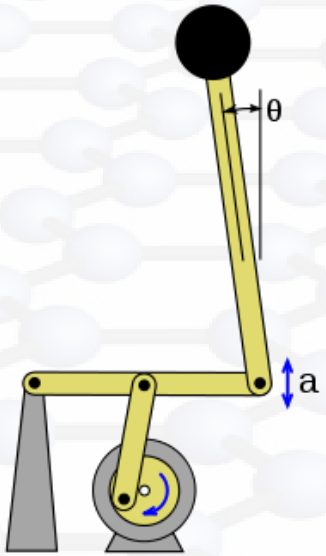

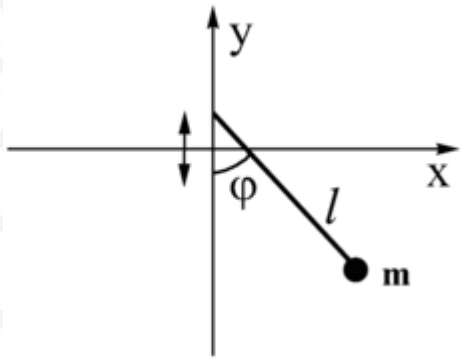

$$\frac{d^2\varphi}{dt^2} = -\frac{g}{l}\sin\varphi - \frac{1}{2}\left(\frac{a\omega}{l}\right)^2 \sin\varphi\cos\varphi \qquad V(\varphi) = -\frac{g}{l}\cos\varphi + \left(\frac{a\omega}{2l}\sin\varphi\right)^2$$

Two minima if $(a\omega)^2 > 2gl$

"Light confinement via periodic modulation of the refractive index", Marrucci et.al., *New Journal of Physics* **15** (2013) 083013

Twisted Light II. Field theory

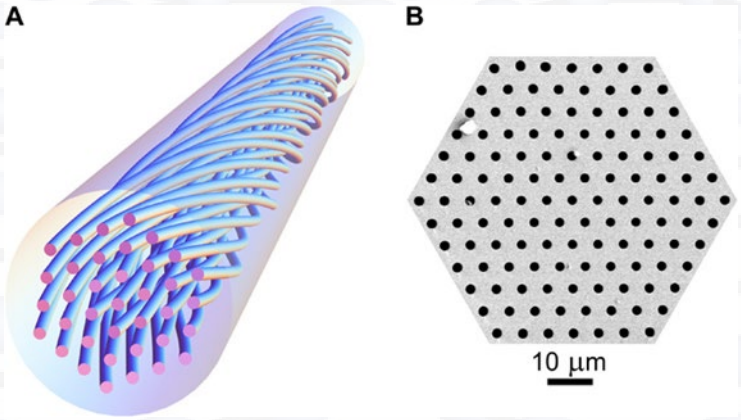

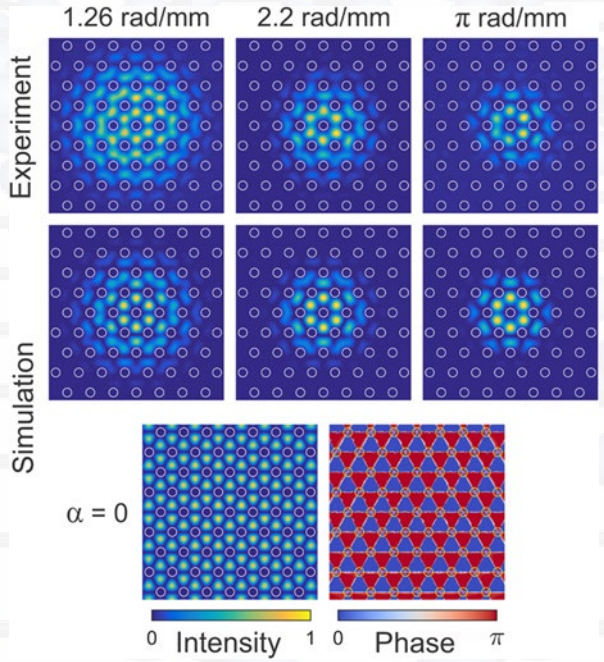

$$2i\beta\frac{\partial\mathcal{E}}{\partial z}+\Delta_{(x,y)}\mathcal{E}-\left(\beta^2-\frac{\omega^2}{c^2}n^2(x,y,z)\right)\mathcal{E}=0$$

$$n(x,y)=1+\Delta cos^2(kx)cos^2(ky)$$

Write eq. in the rotating frame $X=x\cos(\alpha z)+y\sin(\alpha z)$, $Y=-x\sin(\alpha z)+y\cos\alpha z)$ and do averaging

$$2i\frac{\partial\mathcal{E}}{\partial\tau}+i\left(-V\frac{\partial\mathcal{E}}{\partial U}+U\frac{\partial\mathcal{E}}{\partial V}\right)+\frac{1}{\varepsilon}\Delta_{(U,V)}\mathcal{E}-\frac{1}{\varepsilon}\left(\mu-n_{eff}(U,V)\right)\mathcal{E}=0$$

We expect $$\mathcal{E}\approx f(\varepsilon(U^2+V^2),\epsilon\tau)\mathcal{B}(U,V)e^{i\varphi}+\varepsilon\mathcal{E}_1+\cdots$$

Twisted Light: Field theory

$$U=x\cos(\alpha z)+y\sin(\alpha z)\ ,\quad V=-x\sin(\alpha z)+y\cos\alpha z)$$

$$2i\frac{\partial\mathcal{E}}{\partial\tau}+i\left(-V\frac{\partial\mathcal{E}}{\partial U}+U\frac{\partial\mathcal{E}}{\partial V}\right)+\frac{1}{\varepsilon}\Delta_{(U,V)}\mathcal{E}-\frac{1}{\varepsilon}\left(\mu-n_{eff}(U,V)\right)\mathcal{E}=0$$

We expand the field: $\mathcal{E}\approx f(\tau,\varepsilon(U^2+V^2),\epsilon\tau)\mathcal{B}(U,V)e^{i\varphi(\tau,e\left(U^2+V^2\right))}+\varepsilon\mathcal{E}_1+\cdots$

$$C_1\frac{\partial f}{\partial\tau}-C_2f+C_3f\frac{\partial\varphi}{\partial r}=0$$

$$C_1f\frac{\partial\varphi}{\partial\tau}-C_3\frac{\partial f}{\partial r}=0$$

$$r=U^2+V^2$$

$$f(r)=Ae^{-\varepsilon r}\qquad\varphi(r)=\frac{C_2}{C_3}\varepsilon r+\frac{C_3}{C_1}\tau+\varphi_0$$

Adding (constant) Kerr nonlinearity to the model (didn't go beyond this)

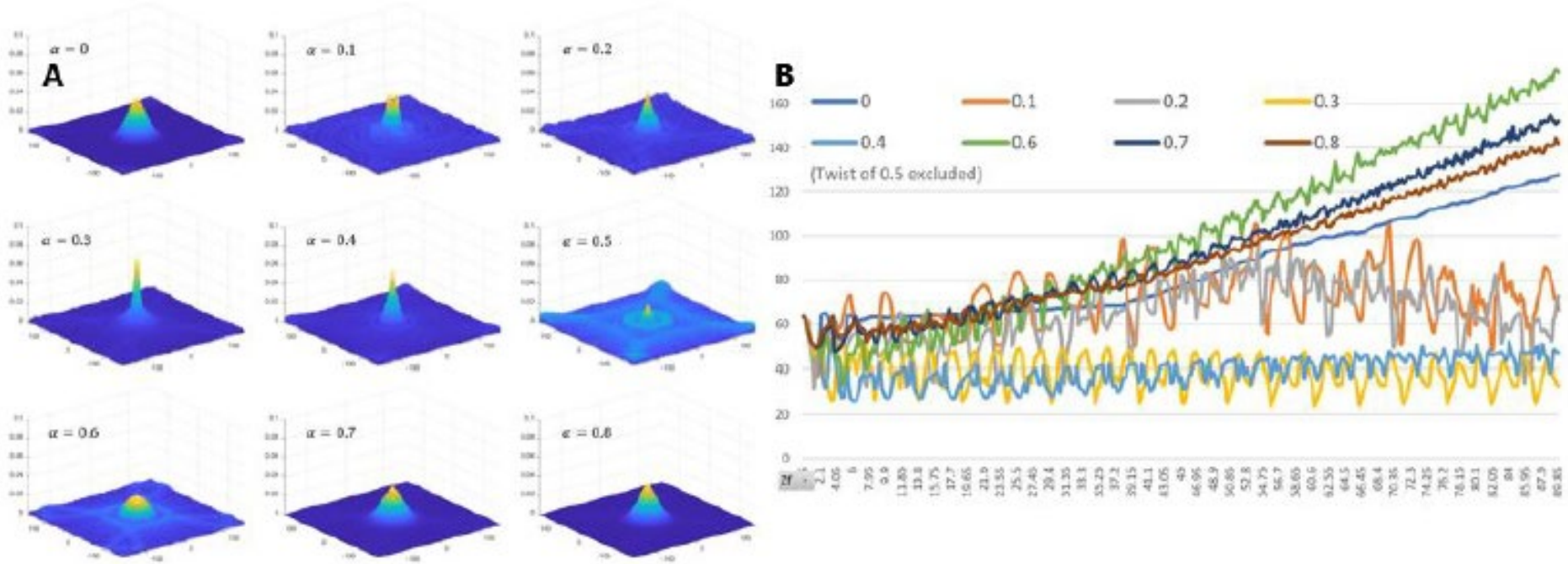

Fig. 1: (A) Mode profiles for increasing rates of twist after propagating a length of 12 rotations for $\alpha = 0.8$. (B) Full width at half maximum measurement as the fields propagate along the z-axis.

Thanks for your attention

- Ross Parker, AA, “Topological Photonics: A Mathematical Perspective”, Notices of the American Mathematical Society 71(8), September 2024
- Ross Parker, Alejandro Aceves, Jesús Cuevas-Maraver, and P. G. Kevrekidis Phys. Rev. E 108, 024214 – (2023)

Research supported by